103

EROSION
RATE

Annealed

Cooling air

7.5.2.2 – a – Changes in the material during incubation

During the incubation period of erosion by liquid impact or cavitation under repeated microjets due to the collapse of bubbles, the changes which occur in ductile materials are essentially the same as during metal fatigue: cold working of initially ductile materials and creation of residual surface compressive stresses.

In the case of 99.999% pure aluminium Vyas and Preece[240] investigated the changes in the surface finish of the metal under the electron microscope, with scanning after 2 seconds exposure to cavitation, and then every two seconds. Cavitation was achieved by an ultrasonic device with a frequency of 20 kHz in which the test specimen was kept stationary in distilled water at 25°C, 115 μm beneath the surface of the vibrator. For a polycrystalline specimen the grain boundaries were below the level after 5 seconds, some grains flowed to the boundaries of adjacent grains and undulations of the surface and of grain boundaries were formed. The behaviour was very similar to that observed by Laurent[241] when studying fatigue in pure aluminium where the movement of the grains away from the surface and the undulations of the grain boundaries had been observed previously. At the end of the incubation period in the tests performed by Vyas and Preece, the cold worked metal became deformed, with rims being converted into ductile lips at the edges of the impact marks; subsequent impacts tended to flatten the rims by breaking them up.

According to Heymann[242] research on the changes in the mechanical condition of the surface as a result of erosion hammering during the incubation period shows rapid initial variation followed by an asymptotic tendency towards a constant condition, as in shot blasting. Plesset and Devine[243] have shown by means of X-rays that in a surface subjected to cavitation, plastic deformation reaches a stable depth almost immediately after the beginning of exposure and remains appreciably constant during the erosion process. In the case of annealed nickel and of electrolytically polished test specimens cavitation-stressed in distilled water at 25°C at a frequency of 20 kHz and an amplitude of 128 μm to 1.59 mm from the surface of the oscillator, measurements of residual stress by deformation after successive dissolutions of the surface have given values of 40 kgw/mm^2 for the residual stress at the surface, being cancelled out only at a depth of 0.35 mm after a 10 second exposure, and of 0.6 mm after 40 minutes exposure, the value at the surface remaining approximately the same.

With a steel containing 0.25% C, 12% Cr, Ni, Mo, V, Beckwith and Marriott[244] showed during erosion tests using a rotating drum and radial specimens that the first stage of the damage for steel tempered at 250°C and tested at an impact velocity of 345 m/s corresponded to "extrusions" along certain crystalline slip planes. Towards the end of the incubation period, the intense plastic deformation of the surface could be described as "smearing" of the surface by the deformation of numerous plastic "extrusions" along the slip lines (Figure 78).
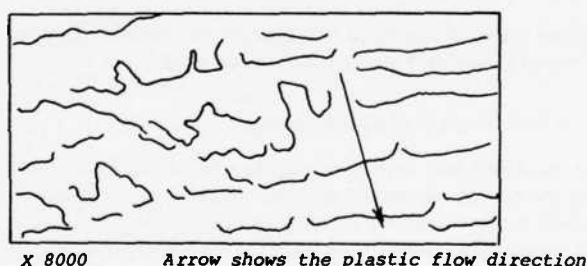

X 8000   Arrow shows the plastic flow direction

Fig.78   Flattening of "extrusions" along plastic slip lines, from a micro-photograph
by Beckwith and Marriott[244]

Several authors have suggested that erosion or cavitation damage occurred by repeated impingement by a process similar to that of fatigue. Figure 79 contains a comparison of the liquid impact fatigue strength curves for aluminium alloys, deduced from the number of impacts, as evaluated during a rotating arm test, and from the calculated impact pressures, with data on the fatigue strength of smooth specimens. The materials investigated by Hoff et al.[245] for rain erosion and by Schütz[246] for fatigue were aluminium and the aluminium alloys used for the construction of aircraft.

With droplets of a diameter of 1.2 mm and a rain density of 1.2×10^{-5} in volume, the erosion incubation times t_i were

$$t_i = a/V^m , \tag{99}$$

with an impact velocity V. The maximum erosion rates were
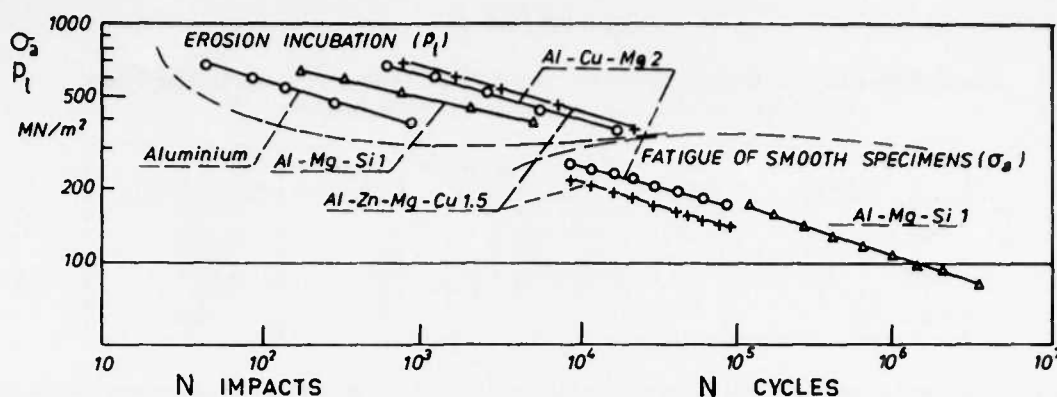
$$(de/dt)_{max.} = b V^n ; \tag{100}$$

Fig.79 Comparison of erosion incubation period curves against hammering pressure with fatigue life curves for aluminium alloys, from Hoff et al.[245]

Schütz's fatigue tests were reflected by

$$\sigma_a = c/V^p .$$ (101)

The values of the exponents m, n and p are given in Table 7.5.2.2 − 1 below.

TABLE 7.5.2.2 − 1

Erosion Incubation, Maximum Erosion Rate and Fatigue Life of Aluminium Alloys, from Hoff et al.[245] and Schütz[246]

Alloys	Erosion		fatigue	
	m	n	p	m, n and p are the
Aluminium	4.9	3.6		exponents of relationships
Al-Mg-Si 1	6.2	4.9	4.7	(99) and (100) for erosion
Al-Cu-Mg 2	5	5.4	5.2	and of (101) for fatigue
Al-Zn-Mg-Cu 1.5	5.2	4.6	6.5	

As in fatigue conditions, certain crystalline phase changes occur as a result of plastic deformation which takes place more readily before a phase change. When discussing a work by Gould[247], Rieger pointed out that in manganese austenitic steels, the transformation from austenite to martensite takes place under impacts, and that the high strength of this steel would seem to be due to the greater hardness of the martensitic phase. It can also be added that the phase change is accompanied by a volume increase which thus introduces residual compressive stresses at the surface. The cobalt alloys investigated by Gould appear to owe their high cavitation strength to the phase change in the cobalt-chromium alloy from the face-centred cubic phase $(200)_{fcc}$ to the compact hexagonal phase $(10\bar{1}1)_{hcp}$. The composition of the stellite 6B specimens was 25% Cr, 4.5% W, 1.5% Ni, 1% Fe, 1% Mn and the remainder, Co. The hexagonal phase proportion was measured by X-ray diffraction; the very rapid transformation at the surface continued in depth during the erosion incubation period. In the erosion debris transformation was complete. After transformation, the material becomes harder and more brittle. The excellent behaviour of the stellite would appear to be due to the phase change which delays the rupture of the metal by permitting considerable plastic elongation and by increasing the hammering pressure level leading to cracking of the metal. A similar transformation is observed in the cobalt alloy L 605 (0.1% C, 20% Cr, 10% Ni, 15% W, 1.5% Mn, 0.5% Si, remainder Co). Gould[247] characterised the rupture energy of the metal by the expression:

$$E_R = \{\sigma_{0.2\%} + (2/3)(\sigma_R - \sigma_{0.2\%})\} .$$ (102)

For the two above-mentioned alloys and the alloys 17-4 PH (0.07% C, 16.5% Cr, 4% Ni, 1% Mn, 1% Si − remainder = Fe) and INCO 718 (0.05% C, 19% Cr, 53% Ni, 19% Fe, 3% Mo, 0.8% Ti, 0.6% Al, 5.2% Cb, 0.004% B). Table 7.5.2.2 − 2 gives the mechanical properties and the stabilised erosion rate in mm/h during cavitation at 20 kHz and an amplitude of 50.8 μm in deionised water at 11 ± 1°C. It will be seen that stellite 6B shows the best behaviour.

Hoff et al.[245] showed, however, that forged stellite was very sensitive to the direction of the rain impact compared with the direction of rolling, deep pitting being observed when a side surface of a test specimen was perpendicular to the velocity of impact of the rain droplets. When applying these findings to steam turbine blade shields, Hoff et al.[245] considered the various practical possibilities of protecting the steel blades with a stellite covering. During deposition by fusion on the surface of the components the stellite becomes compressed after cooling and applies residual tensile stresses to the steel. These residual stresses can be only slightly reduced by annealing after welding, a fact which excludes

TABLE 7.5.2.2 – 2

Tensile Properties and Stabilized Cavitation Erosion Rate of Alloys for Steam Turbine Blades, $f = 20$ kHz, ampl. $= 50.8$ μm, De-Ionized Water, from Gould[247]

Alloys	R_C Hardness	$\sigma_{ult},$ MN/m^2	$\sigma_{0.2\%}$	Elon. %	Rupture "energy" MN/m^2	Erosion rate de_m/dt, mm/hour
17-4 PH	36	1030	930	17	169	0.0082
INCO 718 aged	42	1470	1300	38	538	0.0015
70% cold rolled	52	2000	1990	10	200	0.0022
L 605	23	1030	480	65	545	0.0014
30% cold rolled	47	1480	1450	14	206	0.0014
6B Stellite					156	0.0008

the use of this method of protection for steam turbine blades where the sum of the applied stresses and the residual stresses would exceed the elastic limit. Leading edge shields can still be cast and the edges welded by electron bombardment. During discussion on the above Heymann stated the Westinghouse was using rolled bands which were fitted to the blades by a semi-automatic controlled brazing process; the bands were initially drawn in the direction of rolling but were curved in the other direction to fit the aerodynamic profile of the blades.

7.5.2.2 – b – Erosion and cavitation propagation

As shown in Figure 77, there is a continuous increase in the mean erosion depth e_m after the incubation period t_i; the erosion rate de_m/dt passes through a maximum, then decreases and tends towards a stable value. Quite frequently, erosion tests are not taken far enough to show the stabilisation of the cracking rate after the maximum value has been reached. In practice, a longer service life than that for the maximum erosion rate will be assumed in the case of materials with a very high strength such that the erosion depth remains well below the operating tolerances, e.g. as found by Smith et al.[248] in the case of steam turbine blade shield materials, characterised by the relationship between a stabilised erosion rate and that of a standard tool steel (18% W, 6% Cr, 0.7% C, remainder Fe, hardness number: 630 DPH) taken as a reference. Tool steels, cobalt alloys and tungsten carbides subjected to liquid impacts totalling a quantity of water of 50 kg/cm^2 tended towards final erosion rates of 0.3×10^{-6} to 2×10^{-6} g of metal per g of water. For these materials, the final erosion rate would correspond in practice to a penetration of 2.5 mm; so the maximum value of the erosion rate curve is of little practical importance. This is demonstrated by a cobalt alloy with 31% Cr, 14% W, 1% C which was initially 40 times stronger than the standard tool steel but which was less than 1.5 times as strong after the impact of 100 kg of water per cm^2. Tests show that the erosion rates converge after impacts of more than 40 kg of water per cm^2. The use of a reference material is necessary if the precise conditions of impact are disturbed by the aerodynamic flow and the absolute pressure, such as occurred during the tests by Smith et al. Figure 80 refers to liquid impact tests in a rotating device in which the specimens and the rain ejectors rotate in opposite directions at 12,000 revolutions a minute in a relative-vacuum chamber with an absolute pressure which varies between 50 and 250 mm Hg. At an absolute pressure of 724 mm Hg, Figure 81 shows the development of the weight losses by erosion as a function of time or the weight of liquid projected per cm^2.
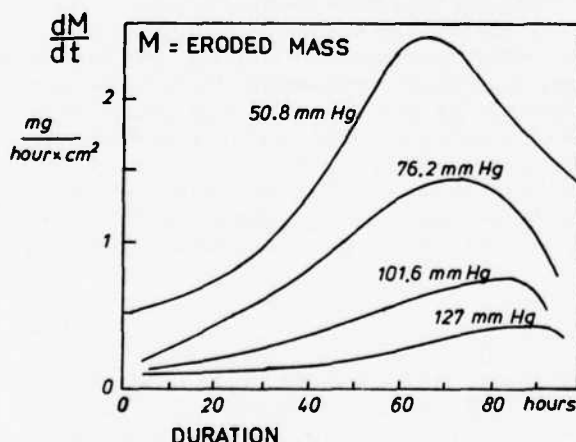

Fig.80   Erosion rate under liquid impact of reference high-speed steel. Influence of the absolute pressure, from Smith et al.[248]
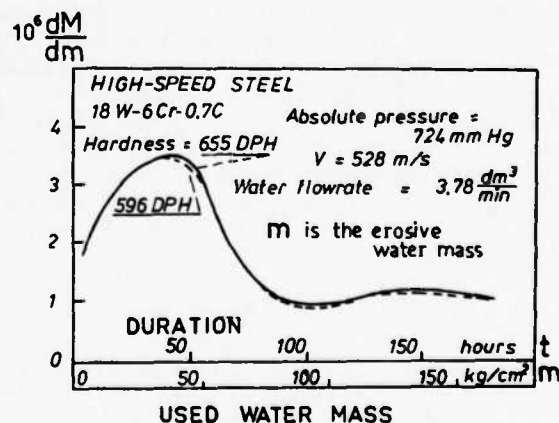

Fig.81   Erosion rate of reference steel under pressure of 724 mm Hg, from Smith et al.[248]

Erosion measurements are performed by weighing the dismantled specimens, the erosion rates being obtained by numerical derivation — a procedure which makes extrapolations very much open to discussion. Starting from a relatively smooth surface and before any crack initiation, plastic deformation causes the build up of residual compressive stresses at the surface. Erosion starts slowly, the erosion rate increasing until the majority of the surface has been damaged, a large number of damaged elements therefore contribute at approximately the same time to the detachment of fragments. The subsequent fatigue development will give rise to a smaller number of fragments with a lower erosion rate after the maximum has been passed. As necessary, other variations in the erosion rate might occur before a stable value is achieved. This phenomenon is fairly general in fatigue conditions. For example, if fatigue crack propagation has been accelerated due to the existence of a local weak point, the material in front of the point of the crack is subjected for a shorter time to the alternating fatigue strains and is more resistant, which reduces the rate of propagation.

When erosion and cavitation tests are carried out in comparable conditions, cavitation erosion and erosion by liquid impact show similar losses and in approximately the same proportions for both types of erosion classification. This was found, for instance, in the multiple liquid impact erosion tests and the cavitation tests performed by Thiruvengadam[249] and referred to in Table 7.5.2.2 − 3.

TABLE 7.5.2.2 − 3

Comparison of Liquid Impact Erosion with Cavitation Erosion, Thiruvengadam tests[249]

	LIQUID IMPACTS $V = 106.75$ m/s jet diameter $= 0.79$ cm specimen diam.$= 0.375$ cm	CAVITATION Specimen diameter $= 0.95$ cm $f = 13.5$ kHz, distilled water double amplitude $= 3 \times 10^{-3}$ cm
Nickel	$(\frac{de_m}{dt})_{max} = 3.5 \times 10^{-3}$ cm^3/h	$(\frac{de_m}{dt}) = 2.8 \times 10^{-3}$ cm^3/hr.
316 stainless steel	2	1
6 Al-4V titanium alloy	0.4	0.9
1100-0 aluminium	70	t00

Nevertheless, any similarity in the behaviour of a material during erosion by repeated liquid impact and erosion by cavitation may be considerably overshadowed and even masked by the predominant influence of vapour tension on cavitation. As pointed out by Schulmeister[250], the temperature has a simultaneous effect on the quantity of gas absorbed in the water and on the chemical and electrochemical reactions which together determine the effect of the temperature on both cavitation erosion and corrosion. If the static pressure remains less than the vapour tension, the bubbles produced do not collapse and there is no erosion. If the difference between the static pressure and the vapour tension is greater than the depression produced by the movement of the vibrator, no bubble is formed. Maximum damage occurs between these two limits. Starting from boiling point, the damage increases with the distance to the vapour tension, that is, with the static pressure if the temperature is constant, since implosion of the bubbles occurs all the more suddenly, the quicker the increase in the pressure of the fluid. Due to the absence of a bubble the upper limit is reached on the oscillator before the bubbles cease to be formed in an undefined environment at rest, the reason for this being the narrowing of the area which produces the bubbles on the front face of the specimen. Reproducible tests can be achieved in the range of conditions in which the damage increases with the pressure.

7.5.2.2 − c − Behaviour during accelerated tests and in service − Effect of corrosion

In addition to the effect of static pressure and temperature on cavitation damage, an important difference in the damage observed during laboratory tests, as compared with behaviour during service, is due to the effect of corrosion. Kallas[251] has summarised the development of ideas and of research results regarding the part played by corrosion in cavitation damage.

In the first place, pitting of the surface, and then the cavernous appearance of oxidised components, such as hydraulic turbine blades and marine propellers, would seem to suggest that there had been a great deal of corrosion. As in the case of the effect of stress on corrosion, some experts have advanced the theory that cavitation erosion is due to the combined action of mechanical and chemical effects, the oxide film protecting the metal being continually torn away by the hammering caused by the implosion of bubbles, so that there is no slowing up of the chemical action which continues at a high rate.

In 1919, however, Parsons and Cook[252] showed that, in the case of steel, the detached fragments were rust, in sea water, and iron in alcohol.

In the same way as for the effect of corrosion on fatigue, consideration must be given to the relative rate at which the metal is damaged under corrosive conditions or as a result of pure mechanical stressing. Although corrosion acts very slowly on sound metal and removes fairly rapidly only the metal which has already become damaged by repeated impact, it is not possible to speak of additional corrosion damage. Laboratory tests are most frequently performed in accelerated conditions as compared with actual service conditions. In agreement with Preiser and Tytell[253] it is possible to conceive of three different areas covered by cavitation erosion, namely, cavitation deformation or fracture, cavitation fatigue and cavitation corrosion, depending on the duration of the test according to the intensity of cavitation. For low cavitation

intensities and long test periods, corrosion might play a significant part, whereas it would be negligible in the usual high speed tests. It was in the field of the cavitation pressures which develop stresses much below the plastic flow limit of the metal that Preiser and Tytell conducted their rotating propeller experiments. With still lower cavitation intensities it is assumed that the cavitation forces can merely destroy the protective oxide film and remove the corrosion products.

Lichtman et al.[254] investigated a number of incidents to ship components in contact with the water and concluded that cavitation was the main cause of damage only in the case of propellers. The damage to tie-rods, rudders and other ancillary equipment was due to corrosion which became more serious as a result of mechanical action. They also came to the conclusion that the slowest laboratory test was performed at a higher speed than that of ships in service and that the damage suffered in service conditions was mainly corrosion accelerated by cavitation turbulence.

One method of increasing the relative importance of corrosion is to apply intermittent cavitation in a device in which the immersed specimen is continuously subjected to corrosive action, as in the tests by Waring et al.[255] in which cavitation increased the damage only in the case of corrosion sensitive materials.

To study the effect of corrosion on cavitation erosion, McGuinness and Thiruvengadam[256] carried out comparative cavitation tests in sea water and in distilled water on specimens made from steel, Al-Mg alloy 5086 H117 and the cupro-nickels 90-10 and 70-30 mounted in the standard ASTM (Ref.257) piezo-electric device. Figure 82 shows some significant results of these tests: for the treated hard steel HY 130, the maximum erosion rate is higher and is reached earlier in sea water (S) than in distilled water (D). This effect of dissolved salt is less pronounced for the semi-hard SAE 1020 steel; it is negligible in the case of the Al-Mg alloy and the cupro-nickels. The authors expressed the assumption that the major effect on a treated and relatively brittle steel was due to the additional embrittling action of hydrogen.
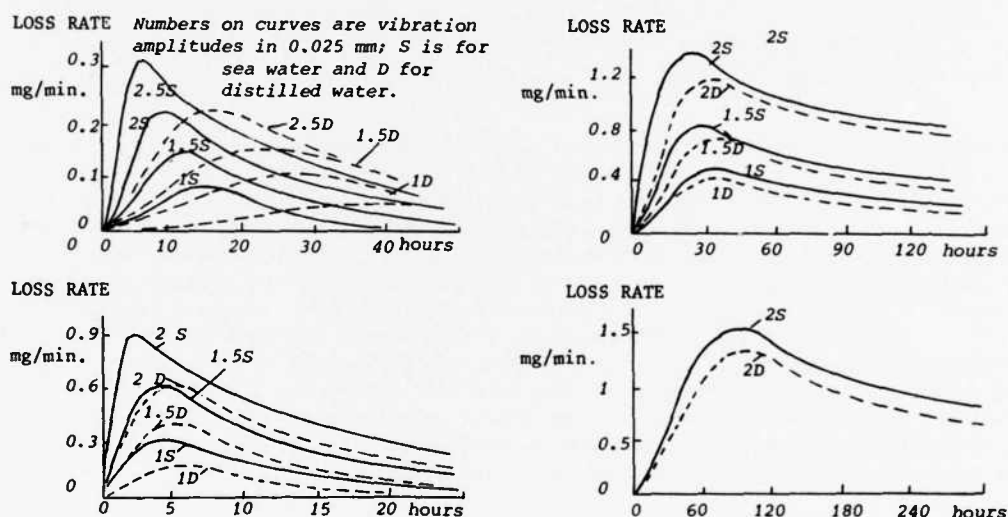
Fig.82   Cavitation mass loss of 15.9 mm diameter specimens in sea water (S) and
in distilled water (D), from McGuinness and Thiruvengadam[256]

Certain practical problems such as reducing cavitation damage in cooling systems of marine Diesel engines have been resolved after systematic tests using corrosion inhibitors. In the prior study of such a problem Schulmeister[250] investigated the loss by cavitation in cast iron, iron, carbon steel and Al-Cu-Mg 2 alloy specimens in baths of (1) distilled water, pH 5.8; (2) hard water, pH 6.1 containing 134 mg of $CaCl_2$ and 156 mg of $CaSO_4$ per litre and (3) three soluble commercial oils a, b, and c, normally used as corrosion inhibitors during machining operations with cutting tools. In certain conditions corrosion inhibitors are an excellent means of protecting components against cavitation. Their effectiveness depends, however, on a large number of influence factors[257]. For example, Figure 83(b) shows that the soluble oil, a, which is very effective on cast iron (Fig.83(a)) attacks the aluminium alloy. Two other similar anti-corrosion soluble oils, b and c, protect aluminium at low temperatures but accelerate erosion at high temperatures. The series of tests carried out by Schulmeister enabled him to draw the following conclusions:

(1) Chlorides and sulphates dissolved in water considerably accelerate cavitation attack in corrosion sensitive materials, such as cast iron or carbon steel; austenite and copper alloys are much less sensitive to salts. The acceleration process is further hastened by oxygen and is greatly affected by temperature and the size of the mechanical stresses.

(2) Corrosion inhibitors can reduce significantly the deterioration of the material; they can also intensify an attack. Their effect depends on the type and concentration of the inhibitor, on the material attacked, on
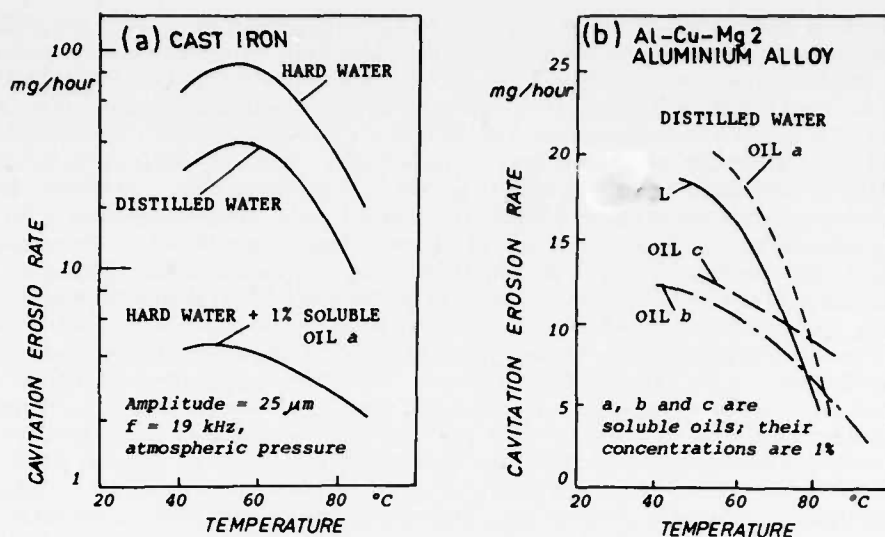
Fig.83   Influence of corrosion inhibiting soluble oils on cavitation erosion of cast iron (a)
and of Al-Cu-Mg 2 aluminium alloy, from Schulmeister[250]

temperature, on the intensity of the mechanical cavitation, on the other substances included in the liquid and
on the age of the inhibitor solution.

(3)   The dissolved gases can accelerate or reduce attack by cavitation or corrosion. The actual effect is determined
by the type and quantity of gas, the material attacked, the composition of the liquid, the temperature and the
intensity of the mechanical cavitation stresses.

The most important fundamental result shown by Schulmeister was that the relationship between the rate of damage
and a particular condition or a particular parameter is very complicated and is determined by the various boundary
conditions and extent of the other influences. It is therefore impossible to make firm useable statements about the
intrinsic significance of a particular influence. Research such as the above examples may merely indicate the particular
importance of an influence or a group of influences, and their inter-relationship. If remedies are sought for a specific
case of damage, special tests suitable for the case in question must be carried out. This type of work has been undertaken
in Darmstadt, aimed at preventing the deterioration of the Diesel engine cooling system. The result gave rise to a series
of recommendations for practical application, including choice of cooling water, a suitable inhibitor, control of the
inhibitor concentration, gas content of the cooling liquid and treatment of aged inhibitor solutions. The in-service value
of these suggestions on treatment of the cooling fluid was proved during field tests carried out by the Federal German
Railways in their ferry, the "Theodore Heuss"[258]. A saving of 250,000 DM a year was effected on the cost price of a
ship's engine.

According to Lichtman[259] cavitation was reduced to a minimum in the cooling water system in Diesel engines by
chemical additions, including corrosion inhibitors, detergents to prevent the formation of foam and wetting agents to
produce a liquid film which adhered to the metal by decreasing the surface tension, factors which affected bubble
formation.

Steller et al.[260] simulated the service conditions for cavitation damage of hydraulic turbine components by placing
cylindrical specimens in the impeller of a "Kaplan" propeller hydraulic turbine in such a way that the front of the
mounting and the surface of the specimen just touched the surface of the impeller. The damage which occurred was
compared with that observed on other specimens, subjected to magneto-striction (frequency: 8.5 kHz, amplitude: 55 μm,
14 mm diameter specimen submerged to a depth of 3 mm in the supply water at 20°C), or tested on a rotating disc at
2890 revolutions per minute, the 30 mm diameter specimens being mounted on a 270 mm diameter circle together with
cavitation exciters consisting of 12 mm diameter pins, the liquid being the supply water functioning in a closed cycle.
An examination of the surface of the specimens and of their micro-sections showed (a) in the magneto-striction tests the
damage corresponds to surface pitting; (b) in the rotating disc cavitation tests the pits are deeper and there are micro-
cracks; finally, at the wall of the force chamber of the turbine, irregular pitting develops in the three dimensions, as well
as cavities the profile of which has become smooth from the simultaneous action of cavitation and corrosion. The grain
joints do not constitute preferential damage points. The conclusion reached is that for the materials tested — annealed
Armco iron, brass with 52% Cu and 38% Zn and cast steel (0.26% C, 5% Mn, 0.4% Si, 0.2% Cr) — corrosion occurs only
in the natural conditions of slow cavitation. The thickness of the worked layer was 10 times greater in natural cavitation
than during magneto-striction, which may account for the slower development of the microcracks. The authors mention
the existence of cases in which materials considered to be excellent, according to the results of accelerated tests, turned
out to be of mediocre quality in actual conditions of use.

In certain problems involving both corrosion and erosion by liquid impact of water droplets, the conditions are sometimes such that corrosion attacks act reciprocally on one another and that the parameters of the problem, as yet not fully understood, cannot be simulated during tests of a simple type. It was these conditions for example which were described by Van der Horst and Sloan[261] relating to the damage in service of a converted gas cooler in an ammonia production factory. The gas came from the conversion by catalysis of $CO_2 + H_2O$ into $CO + 2H$ and contained hydrogen, CO_2, nitrogen and water. The cooler removed the water by condensation. The gas entered the inlet at a temperature of $127°C$ and a pressure of $1650 MN/m^2$; the outlet temperature was $50°C$ and the pressure $1630 MN/m^2$. It contained 13.2 mol per cent of water at the inlet as against 0.7 mol per cent at the outlet. The partial pressure of the CO_2 was $269 MN/m^2$. The water circulated in finned tubes, and the gas, in the cooler around the tubes. The condensation water, however, remained between the fins spaced at 1 mm intervals, thus eliminating any advantage afforded by the fins. The first finned tubes were made of brass but were then replaced by carbon steel tubes. The steel fins were then attacked and disappeared quickly. Incidentally, re-calculation of the heat transmission showed that the fins served no useful purpose. The surface of the corroded finned tubes was completely covered with rhombohedral crystals of ferrous carbonate. It is known that, when dissolved in water, CO_2 corrodes carbon steel. At medium temperatures, velocities and pressures, this type of corrosion ceases of its own accord since, in the absence of oxygen, the corrosion product is a ferrous carbonate which is only very slightly soluble in water ($0.0067 g/100 cm^3$ at $25°C$). The much more soluble ferrous bicarbonate would appear to be formed at partial pressures of CO_2 and at much higher temperatures. The author then calculated the gas velocities which at the most were 51.8 m/s and therefore less than the threshold values quoted by Thiruvengadam[215] or Heymann[230] for liquid impact erosion of carbon steel. There is therefore a mutual reinforcing effect between erosion and corrosion.

7.5.2.3 Data on Erosion Resistance

We have already discussed the correlation between the resistance to sand erosion and the resistance to cavitation of materials used in the construction of hydraulic turbines and marine propellers (see 7.5.1.1 – a). It has been shown that, generally speaking, damage is the result of plastic deformation which governs the rupture of components or the development of fatigue effects, due to impact by abrasive grains, liquid drops or cavitation microjets. The existence of a common damage mechanism, with different levels of the extent of the plastic deformation occurring after each impact explains the possible ways of correlating resistance to various forms of erosion with the static resistance and with the fatigue resistance. As in the case of correlations of the wear resistance with the modulus of elasticity, the present correlations are very rough and are influenced by the effect of the parameters more specifically related to each material.

7.5.2.3 – a – Classification lists of erosion resistant materials

In 1962 Rheingans[262] discussed damage to hydraulic turbines resulting from erosion by foreign particles in suspension such as sand, clay or ice particles and, in the area of hydrodynamic depression, the formation of pits resulting from cavitation and making their appearance in the high velocity areas where there are changes of direction or flow separation and where vapour bubbles form at rates of 10,000 to 20,000 a second. The complete life of a bubble is a few microseconds; it collapses, producing a point pressure of 350 to 700 MN/m^2. The material in contact is destroyed immediately or as a result of fatigue under the repeated action of the bubbles. A direct relationship exists between the flow velocity and the pressure for the initiation of bubble formation:

$$K_i = \frac{p - p_v}{\rho V^2/2} , \tag{103}$$

in which K_i is the number for the initiation of cavitation, p is a characteristic pressure of the system, p_v is the vapour pressure of the liquid and ρ is its specific mass, V being a characteristic velocity of the system. For hydraulic turbines the cavitation discriminant is used again:

$$\sigma = \frac{H_b - H_s - H_v}{H} \tag{104}$$

where, in metres for the height of the water, H_b, H_s, H_v and H correspond respectively to the turbine inlet pressure, the outlet suction height, the vapour tension for the temperature and $H = \rho V^2/2$ is the dynamic pressure.

From his experience of the behaviour in service of hydraulic turbines, accumulated from 35 years of use, Rheingans[263] published a qualitative classification list of a number of materials based on their actual behaviour (List 1 in Table 7.5.2.3 – 1). A second list was drawn up[262] from cavitation tests performed on vibrating devices and on various test machines giving quantitative results which were hard to compare but which nevertheless made it possible to classify the materials.

It will be seen that there is an excellent correlation between the two classifications, probably due to the fact that corrosion plays only a very small part in the damage to materials originally chosen for their high corrosion resistance, and justified by the common erosion mechanism, by the entrained particles and, in cavitation, damage by repeated impact pressures.

TABLE 7.5.2.3 – 1

Qualitative Classification Lists of the Erosion Resistance of Materials from Service Behaviour
in Hydraulic Turbines (List No.1) and from Cavitation Tests (List No.2), from Rheingans[262]

List No. 1 . Service behaviour	List No. 2 - Cavitation tests
1 Stellite	1 Stellite
2 17-7 Cr-Ni Stainless steel	2 17-7 Stainless steel, welded
3 18-8 Cr-Ni Stainless steel, welded	3 18-8 Stainless steel, welded
4 Ampco no. 10, welded	4 Bronze al. Ampco no. 18, welded
5 25-20 Cr-Ni steel, welded	5 Bronze al. Ampco no. 18, casting
6 2-24 eutectic-xyron, welded	6 Ni-Al bronze, casting
7 Ampco bronze, casting	7 18-8 stainless steel, casting
8 18-8 stainless steel, casting	8 13% Cr steel, casting
9 Ni-Al bronze, casting	9 Mn bronze, casting
10 13% Cr steel, casting	10 Carbone steel, casting
11 Mn bronze, casting	11 Bronze, casting
12 Sprayed 18-8 steel (coating)	12 Cast iron
13 Cast steel	13 Sprayed 18-8 steel (coating)
14 Bronze	14 Rubber
15 Rubber	15 Aluminium
16 Cast iron	
17 Aluminium	

Reiger[264] has compared the behaviour of various materials in:

(1) impact tests by liquid droplets in a rotating arm device under uniform test conditions: impact velocity
$V = 410$ m/s, 1.2 mm diameter droplets, rain density: 1.1×10^{-2} droplets/cm^3 at 25°C;

(2) cavitation tests performed in a magneto-striction device at a frequency of 20 kHz with specimens fixed to
the vibrating head, to investigate cavitation resistance.

Figure 84, taken from Table 1 of Reference 264, shows the correlation between the durations of the incubation
periods (Fig.84(a)) and between the maximum erosion rates (Fig.84(b)) obtained in rain erosion tests or in cavitation
tests. These correlations are fairly weak, even if we exclude glass and the polycarbonate "Makrolon"; this implies some
difficulty in predicting the resistance to rain erosion from the results of cavitation tests.
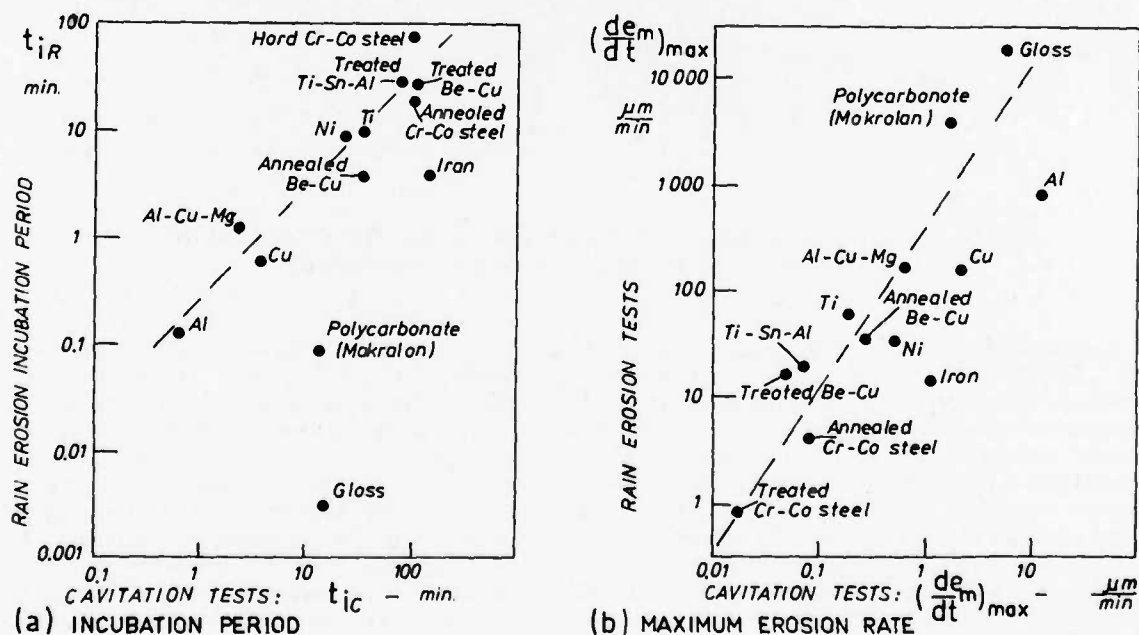
Fig.84   Correlation of incubation period and maximum erosion rate experienced in
rain erosion with those of cavitation in water, from tests of Rieger[264]

According to Speidel and Keser[265] erosion damage in 12% chromium steel tubes used in steam turbine installations
is due to the growth of cracks which originate from erosion pits. The cracks are transgranular compared with austenite
grains. The problem of the erosion resistance of these steels is complicated by their susceptibility to stress corrosion and

to corrosion fatigue. An early investigation of the mechanical properties of this type of steel and of their correlation with erosion resistance had been made by Beckwith and Marriott[244] (see 7.5.2.2 − a) on a steel containing 0.25% C, 12% Cr, Ni, Mo, V, austenitised at 1050°C, air cooled and tempered for 1 hour at one of the following temperatures: 150, 250, 450, 550, 600 or 650°C. They had determined the fracture toughness K_{Ic} by slow bending of specimens pre-cracked in fatigue conditions. The erosion tests were carried out by repeated impacts of liquid jets hitting specimens mounted radially on a rotating drum. Table 7.5.2.3 − 2 below gives the results of these tests.

TABLE 7.5.2.3 − 2

Strength Properties of a 12% Cr Steel for Various Tempering Temperatures, from Beckwith and Marriott[244]

Tempering temperature °C	Hardness HV 30	$\sigma_{0.2\%}$ MN/m^2	$\sigma_{ult.}$	Reduction in area %	Charpy Impact test	K_{Ic} MN/m$^{3/2}$	Strain-hardening exponent n
150	610	921	1706	5	6	60	0.09
250	545	932	1661	28	17.5	98	0.13
450	512	1018	1434	47	8	66	0.17
550	595	1041	1730	27	4.5	63	0.10
600	570	1142	1470	43	4	61	0.09
650	385	776	1041	37	7.5	98	0.11

Figure 85 shows the progression of losses by erosion under repeated liquid impact, and the gradual reduction of the erosion rate with the test duration. As in the case of the mechanical strength properties, the losses by erosion depend a great deal on the tempering temperature and pass through a maximum during tempering at 450°C, return to a low value during tempering at 550–600°C and increase again during tempering at 600°C. This phenomenon should be compared with the known instability of austenite which promotes plastic deformation, the hardness assuming a higher value if the austenite/martensite transformation takes place locally at the point of impact.
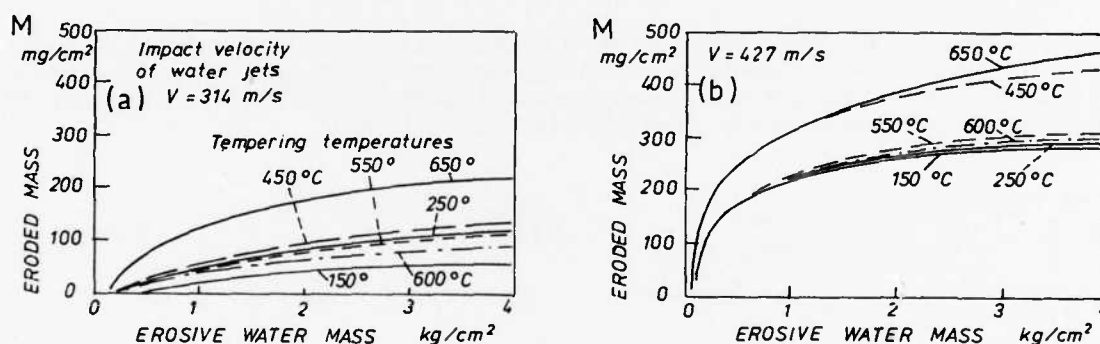
Fig.85   Influence of tempering temperature on erosion losses of a 12% Cr steel undergoing repeated impacts with liquid jets, from Beckwith and Marriott[264]

Speidel and Keser[265] have made a more complete study of the American type 420 martensitic stainless steel with 0.2% C, 12% Cr, 1% Mo, 0.3% V and 0.5% Ni. After annealing at 1060°C for a 0.5 hour, cooling in air and tempering for 10 hours at various temperatures, the investigation included measurement of the tensile strength characteristics and determination of the incubation periods and the maximum erosion rates following the erosion tests performed on the "Dornier" rotating arm with a normal impact velocity of V = 410 m/s and 1.2 mm diameter droplets with a volume concentration of 1.2×10^{-5}. The development of the erosion characteristics, that is, the incubation time t_i and the maximum erosion rate $(dM/dt)_{max.}$ as a function of the tempering temperature, is shown in Figure 86. Again, slightly variable values are obtained for tempering temperatures between the ambient and 500°C; beyond this temperature the incubation time decreases considerably and the erosion rate increases very quickly. Figure 87 contains the fracture toughness values K_{Ic} and the stress corrosion cracking rate in distilled water, and a constant value for the stress intensity factor K (45 MN/m$^{-3/2}$) applied to DCB (Ref.266) type specimens for various values of the tempering temperature. There is some degree of correlation between the reduction in ductility, as measured by the reduction in the tensile elongation at break, and that in the fracture toughness K_{Ic}, with an increase in the stress corrosion rate during tempering at 400 to 500°C, but no clear correlation with the resistance to erosion. The cracks observed in the final phase of the rain erosion are transgranular while the stress corrosion cracks are intergranular; stress corrosion is therefore not the mechanism responsible for rain erosion cracks.

In fatigue there is a correlation between the peak-to-peak variation $\Delta K = 2K_a$ of the stress intensity factor and the crack propagation rate in mm per cycle. For high values of ΔK, tests in a vacuum of 10^{-5} mm Hg and a frequency of 2.3 Hz, the fatigue propagation rate measured for different tempering temperatures is in agreement with the expression

Fig.86 Incubation period and maximum rain
erosion rate of a 12% Cr steel at an impact velocity
of 410 m/s, from Speidel and Keser[265]

Fig.87 Maximum stress-corrosion crack propagation
rate and critical fracture toughness,
from Speidel and Keser[265]

$$\Delta a/\Delta n = 6\left(\frac{\Delta K}{E} - 2.7 \times 10^{-5}\right)^2 \Big/ \left(1 - \frac{\Delta K}{K_{Ic}}\right), \tag{105}$$
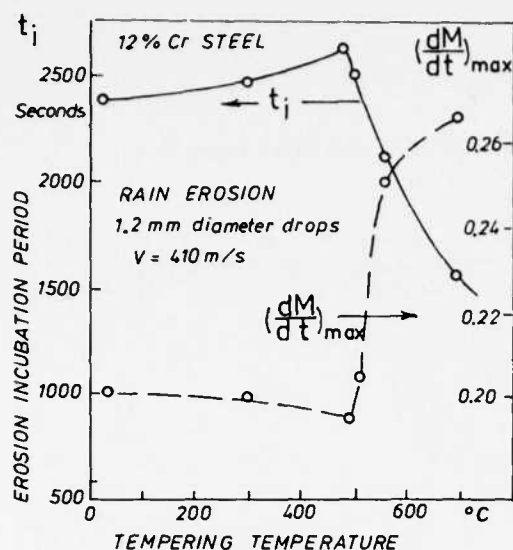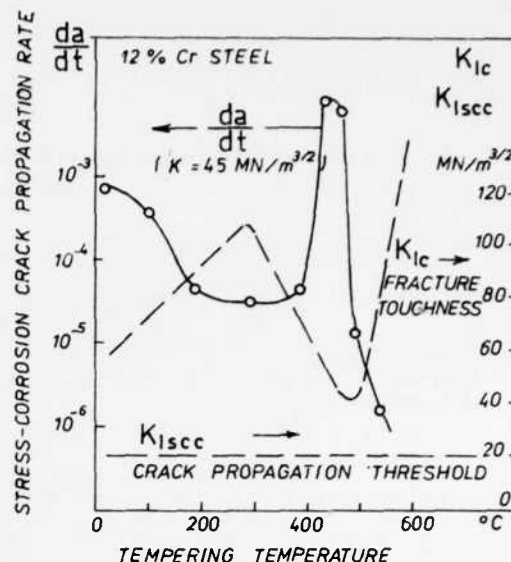
in which the critical value for static fracture, K_{Ic}, occurs by the Forman correction: at low values of the stress intensity factor, the tempering temperature does not appear to have any effect on the fatigue crack rate. Figure 87 also shows that the threshold value K_{Iscc} for initiation of stress corrosion cracking is not related to the heat treatment.

Two distinct correlations emerge from all the tests performed: a linear correlation between the alternating bending fatigue limit and the tensile strength of smooth, polished specimens subjected to tests in air at ambient temperature, and a linear correlation between the rain erosion incubation period and the 0.2% tensile yield point. Taking into account the more approximate correlation between the tensile strength and the yield point, a correlation therefore exists between the erosion incubation period and the development of plastic deformation leading to fatigue rupture. The instability of the residual austenite and the creation of corresponding residual compressive stresses in the area of the surface subjected to erosion impact is, however, a fairly complex function of the tempering temperature which affects in different ways the surface indentation of the edges of the craters produced by impacts, and the propagation in depth of the fatigue cracks which originate at the surface.

The damage, measured by the ratio of the erosion rate to the flow of the erosive liquid, first of all increases very quickly with the covered proportion of the surface, reaches a maximum and then decreases asymptotically tending towards a very low value which is only very slightly dependent on the heat treatment (see Figures 85(a) and 85(b)). In the final state with a very low erosion rate, the weight losses are slight, although deep cracks may compromise the use of actual components.

The use of 12% Cr, Mo, V martensitic steels (American types 410, 420, 422 and 436) is based mainly on the very low general corrosion rate for heat treatments giving a static strength and a fatigue strength of the same order as the slightly alloyed carbon steels which are very susceptible to oxidation. Their service use is, however, compromised by corrosion with large cavities, stress corrosion and hydrogen embrittlement[267].

Gould[268] carried out cavitation tests using a piezoelectric device at a frequency of 20 kHz in which the 12.7 mm diameter specimens were screwed on to the moving horn. The tests, made on stainless martensitic steels, an austenitic steel, a Ni-Cr INCO 82 T alloy, a Cr-Co stellite 6B alloy, titanium alloys, pure molybdenum, 1100 aluminium and magnesium, were performed at one or more values of the vibration amplitude of the specimen. The test conditions and results are contained in Table 7.5.2.3 – 3. In all cases the erosion rate increased very rapidly after the incubation period, reached a maximum and then tended asymptotically towards a stablised value which was achieved relatively quickly because of the high vibration frequency. The Table merely gives the stablised value of the erosion rate. It can be oberved that the intensity of the stabilised erosion rate is proportional to the square of the amplitude. For the same hardness value the titanium alloys arc superior to the steels. The best material is stellite 6B. In addition, examination under the electron microscope revealed fatigue marks in the eroded area of a specimen made from the IMI 680 titanium alloy.

TABLE 7.5.2.3 – 3

Comparative Cavitation Tests of Materials Used in Blades of Aircraft Engine Compressors and Turbines, from Gould[268]

Material	Composition %	ρ $\frac{g}{cm^3}$ DENSITY	REDUCTION IN AREA %	BRINELL HARDNESS	$\sigma_{ult.}$ MN/m² (estimated from hardness)	$\sigma_{.2\%}$ MN/m²	Peak-to-peak vibration amplitude μm	Stabilized erosion rate in mass g/hour	in depth† mm/hour
Martensitic steels									
12%Cr-Mo (B50A 332A)	12Cr-0.10C-0.20Mo	7.7	60	236	690	483	35.6	0.0097	0.01
							104.1	0.043	0.044
							124.5	0.053	0.053
				480	1655		35	0.0021	0.002
							95.3	0.0075	0.077
Maraging 455 steel	11.3Cr-8.8Ni 1.3Ti	7.7	75	465	1608		35	0.0018	0.0018
Maraging X15 steel	15Cr-20Co-2.8Mo	7.7	75	465	1656	1550	35	0.0018	0.0018
							95.3	0.0059	0.0060
Maraging 10-10-2	10Cr-10Ni-2Mo	7.7	71	380	1346	1311	35	0.0042	0.0043
12Cr "ausformed"	12Cr-0.5Mo-V	7.7	68.5	330	1118	890	35	0.0038	0.0039
				345	1166	945	35	0.0038	0.0039
12Cr 434	12Cr-1Mo-0.2C-0.2V	7.7	69	295	932	656	35	0.0042	0.0043
12Cr 481	12Cr-1Mo-0.22C-0.25V	7.7	69	315	1014	690	35	0.0029	0.0029
Tool steel	11.7Cr-1Mo-1V-1.5C	7.7	82.5				35	0.00051	0.0005
Austenitic steel									
SAE 347	18Cr-11Ni-1Cb	8	34	85	483	345	35	0.0048	0.0047
			60	230	828	621	35	0.0075	0.0074
Refractory alloys									
INCO 82T	67Ni-18Cr-3Cb-3Fe	8.14	48	160	656	393	35	0.0011	0.0106
							89	0.050	0.048
STELLITE B	3Ni-2Si-28Cr-1.2C-reste Co	8.38	70	360	1035	621	53.3	0.00068	0.00064
							95.3	0.0035	0.0033
Titanium alloys									
A 110 AT	Ti-5Al-2.5Sn	4.46	69	342	925	856	35	0.0017	0.0030
							57.2	0.0028	0.0050
							95.3	0.0055	0.0097
							127	0.0125	0.022
							146.1	0.017	0.030
V3275	Ti-2Ni	4.54	48	141			89	0.0125	0.021
D6860	Ti-7Al-2.5Mo	4.46	66	290			89	0.0055	0.009
V3272	Ti-8Mo	4.54	62	230			89	0.0100	0.0174
V3278	Ti-2Al-4Zr-4Mo	4.5	61	235			89	0.0082	0.0142
D9760	Ti-6Al-4V-low O	4.44	62	230	966	897	89	0.0070	0.013
D1184	Ti-6Al-4V	4.44	66	297	966	897	89	0.0067	0.012
IMI 680	Ti-2.2Al-4Mo-11Sn-0.2Si	4.85	72	402	1311	1187	35	0.00154	0.0024
Maraging steel nitrided 482°C 48 h at: 454°C	10Cr-10Ni-2Mo	7.7	86				35	0.005	0.005
							35	0.0056	0.006
Pure Molybdenum	wrought recrystaled	10.2	53				35	0.0089	0.007
							35	0.0115	0.009
1100 Aluminium	wrought	2.7	61				35	0.032	0.093
Magnesium	wrought annealed	1.76	92				35	0.0087	0.039
							35	0.0094	0.041

† Values computed by assuming a uniform erosion on the front surface of the 12.7mm diameter specimens.

This Table can be supplemented by Table 7.5.2.2 — 2, from more recent studies by the same author[247] using the same piezoelectric device but with thin specimens (1.27 mm thick) brazed on to a mounting screwed into the head of the vibrator.

Cobalt and chromium alloys of the stellite type, used as welded shields for steam turbine blades, were also investigated by Hoff et al.[245] from the point of view of rain erosion. A direct comparison of behaviour as between the erosion due to cavitation impacts and that caused by rain drop impacts is very difficult to achieve except in the form of fairly imprecise correlations, such as those shown in Figures 84 and 85 for incubation periods and maximum erosion rates for various materials, between the values arising out of the rain erosion tests and the cavitation tests in water. Any direct comparison is impossible since, although it is possible to determine the impact pressure and the diameter of the craters and their number per unit area in the repeated rain drop impact erosion tests, the values of these parameters are not known in the cavitation tests, where the main indicators in the stress conditions are the pulsation frequency, its peak-to-peak amplitude, the nature of the liquid and its static pressure.

Figures 88 and 89 show the increase in the erosion depth in relation to the test duration respectively for cavitation and rain erosion, in the case of titanium alloys and some other alloys, after Hoff et al.[245].
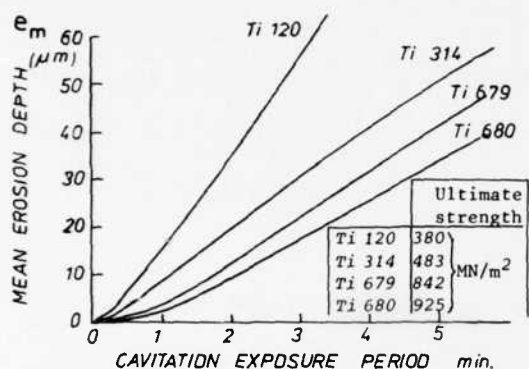

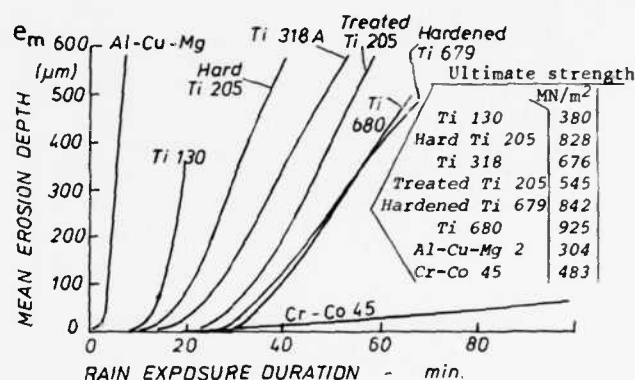Fig.88   Mean cavitation erosion depth for titanium alloys, from Hoff et al.[245]

Fig.89   Mean rain erosion depth for titanium alloys (V = 410 m/s), from Hoff et al.[245]

7.5.2.3 — b — Effect of liquid properties on cavitation erosion

The use of liquid metals as power transmission agents or for cooling purposes in atomic reactors and in gas turbines has led to cavitation damage in the liquid metal circulating system. Using a magneto-strictive oscillator at a frequency of 25 kHz, Young and Johnston[269] investigated the cavitation wear of various steels or refractory alloys in liquid sodium at $427 \pm 5.5°C$ and mercury at $149 \pm 16.7°C$, the vapour tensions being 0.1 bar and the vibration amplitude 44.45 μm to within ± 1.3 μm. The tests were performed in a heated chamber under a partial vacuum. The 14.3 mm diameter specimens were screwed on to the end of the amplifier horn (see Figure 90(a)) which was fixed to the core of the oscillator and provided with a water-tight skirt around the tank containing the liquid metal. During the discussion Wilson, R.W. drew attention to the fact that accelerated cavitation tests minimise the part played by corrosion, although in actual service conditions this may increase the effect of the mechanical damage suffered. Even non corrosive liquids may react with metals as a result of the local pressure and high temperatures reached during collapse of the cavitation bubbles. The composition of the metals used and the results of the cavitation tests are contained in Tables 7.5.2.3 — 4a and 4b.

Figure 90(b) shows the variation in the erosion rate with the period of exposure to cavitation in liquid sodium at $427°C$ (vapour tension $\approx$ 1 atmosphere). We again find the maximum already noted in other cases and a very clear tendency to stabilisation of the erosion rate. Figure 91 refers to an attempt by the author to show the correlation between the tensile strength properties and the corrosion strength, measured by the time required to erode 1 mm^3 of the material at the surface of a 14.3 mm diameter specimen when the corrosion rate has been stabilised at its lowest value. It will be seen that stellite B is outside this correlation by a value 6 times higher, for which the explanation is the same as in Gould's tests[247].

In a series of more recent tests Young and Johnston[270] examined the influence of the static pressure of the liquid on cavitation losses in liquid sodium at various temperatures. The tests were made on 14.3 mm diameter L-605, stellite 6B and AISI 316 steel specimens attached to the end of a magneto-strictive oscillator vibrating at 25 kHz with a peak-to-peak amplitude of 44.5 μm, the surface of the specimens being 3.3 mm below the surface of the liquid. The heated water-tight tank containing the liquid sodium had previously been emptied of air at a partial pressure of 10^3 mm Hg $(0.13 N/m^2)$ and then filled with argon the pressure of which was controlled to within 1.7×19^3 N/m^2 for each test.

TABLE 7.5.2.3 – 4a

Composition and Treatment of High-Temperature Resistant Materials Subjected to Cavitation Tests in Liquid Sodium or Mercury by Young and Johnston[269]

Materials	Treatments	Composition , per cent													density
		Fe	Ni	Co	Cr	Mo	W	Cb	Ti	Al	C	Mn	Si	Others	
Stellite 6B	Sol. 1230°C air quenched	3	3	rem.r	30	1.5	4.5			1.4-1.8	1.1	2	2		8.38
René 41 (AMS 5712)	Sol. 1079°C rapid quenched	5		10-12	18-20	9-10.5	14-16		3-3.3		.12	.1	.5	Boron: .003 to .01	8.25
L 605 (AMS 5759	Sol. 1230°C Water quenched	3	9-11	rem.r	19-21		0.2-1				.05-.15	1-2	1		9.13
Hastelloy (AMS 5754	Sol. 1177°C rapid air quenching	17-20	rem.r	0.5-2.5	20.5-23						.05-.15	1	1		8.23
A-286 (AMS 5736	Sol. 1010°C Water,16hr.718°C	rem.r	24-26		13.5-16				1.9-2.3	.35	.08	1-2	.4-1	.3 V .01 boron	7.94
Inconel 600 (AMS 5665)	annealed	6-10		1	14-17			1	0.5		.15	1	.5	.5 Cu	8.43
Stainless AISI 318	annealed	rem.r	13-15		17-19			0.8			.08	2.5	I		7.99
AISI 316 (AMS 5648	annealed	rem.r	12-14		17-19						.08	1.25-2	1	.5 Cu	7.98
Sicromo 9M	ann.d 1hr.954°C 1 hr.732°C, air	rem.r			8-10						.20	.35-.65	1		7.61

TABLE 7.5.2.3 – 4b

Results of Cavitation Tests in Liquid Sodium and Mercury of the Materials Listed in Table 7.5.2.3 – 4a

	Volume losses (mm^3) after (hours)				Stabilized erosion rate	Surface roughness , μm , after (hours)			
In sodium at 426°C	1	2	3	4	mm^3/hour	1	2	3	4
Stellite 6B		0.04	0.13	0.39	0.5				1.27
René 41		0.20	1.12	2.42	1.3	0.38	1.01	1.65	2.16
L 605		0.22	1.25	2.58	1.4	0.9	1.4	1.9	2.5
Hastelloy X	0.66	3.10	5.78	8.14	2.4				
A-286	1.40	4.70	7.67	10.4	2.8				
AISI 318	2.7	6.40	10.3	13.4	3.1				
AISI 316	2.9	7.16	11.8	15.9	4.1	2.03	2.5	2.9	3.05
Annealed Sicromo 9M	6.4	15.5	24.7	33.9	9.2	6	7.4	8.13	8.51
In mercury at 149°C									
Stellite 6B	0.34	0.75	1.28	1.81	0.6	1.65	2.5	3.17	3.8
Hardened Sicromo	1.07	3.45	6.8	10.5	3.4	3.94	6.6	11.4	17.8
L-605	1.12	4	7.6	11.3	3.6	6.7	9.27	13.3	19.05
Hastelloy X	5.02				8.2	8.2	13		
Annealed Sicromo 9m	18.2				17.4	17.4	19.4		

Figures 92(a), (b) and (c) show the development of the mean erosion rate in mm³/h for each of the materials. The mean rate of propagation of the erosion in depth, de_m/dt, would be obtained by dividing the erosion rate by the area of the front face of the specimen, $A = 169.6$ mm².

With increasing values of the static pressure the maximum erosion rate increases to a greater extent than the subsequent stabilised minimum value and occurs earlier. Stellite 6B has greater erosion resistance than the other two alloys and can maintain this resistance in the event of a static pressure increase.

The dynamic pressure generated by the vibrations is governed by the amplitude, the frequency and the viscosity of the liquid opposing its flow; it is zero at the edge of the front face of the specimen and there is no uniform pattern in the cavitation damage, which is non existent at the periphery. To allow for this factor Young and Johnston corrected the stabilised erosion rate, corresponding to the minimum erosion rate after the first maximum value, by multiplying the uncorrected values in the Figure by the ratio of the apparent area of the front face of the specimen to the area actually eroded.

The corrected stabilised erosion rate, the variation of which is shown in Figures 90 to 93, corresponds to the product of the severely eroded area of the face of the specimen and the mean rate of penetration of the erosion over this area, i.e.: *corrected erosion rate* = $A_{eroded} \times de_m/dt$.

EROSION
RATE
$\frac{mm^3}{hour}$

Annealed
9M Sicromo

427 °C

316 AISI
318 AISI
600 Inconel
A-286
X Hastelloy
L-605
René 41
6B Stellite

0   80   160   240 (min.)
EXPOSURE DURATION t

(b)

Cooling air

Excitation by
magneto-striction

Amplification horn

Tightness

Specimen

Liquid metal

(a)
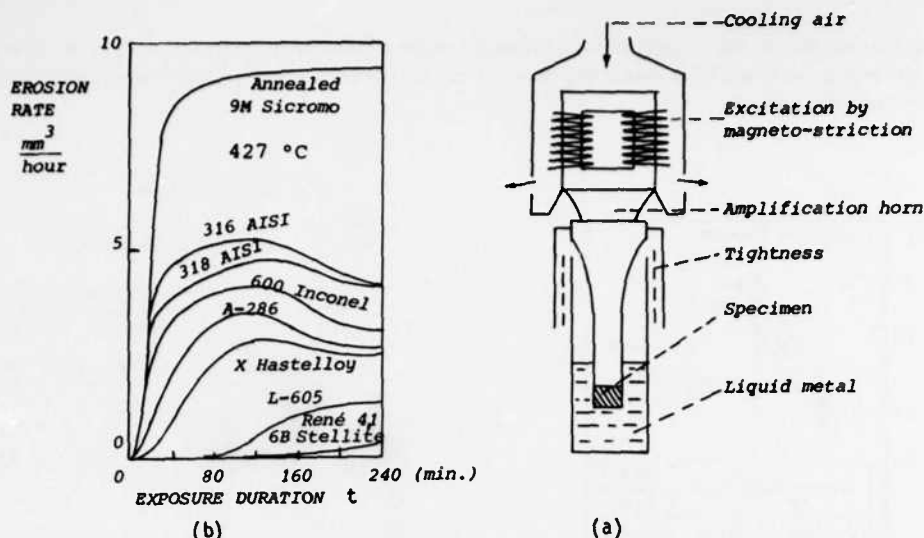
Figure 90

(a) Cavitation test apparatus using liquid metals
(b) Test results with liquid sodium. From Young and Johnston[269]

TIME PERIOD TO ERODE ONE mm^3 AT STABILIZED CAVITATION RATE
(hour)

$\sigma_{0.2\%}$ $\sigma_{Ult.}$ MN/m^2		El. %
489	952	29
241	821	75
324	690	50
635	945	21
200	607	49
193	483	40

to 2 hr./mm^3
6B Stellite

L 605

Hastelloy X
600 Inconel
A-286
316 AISI

0   100   200   300   400 MN/m^2

STRAIN "ENERGY" = ($\sigma_{0.2\%}$ + $\sigma_{ult.}$) (tensile elong.)/100
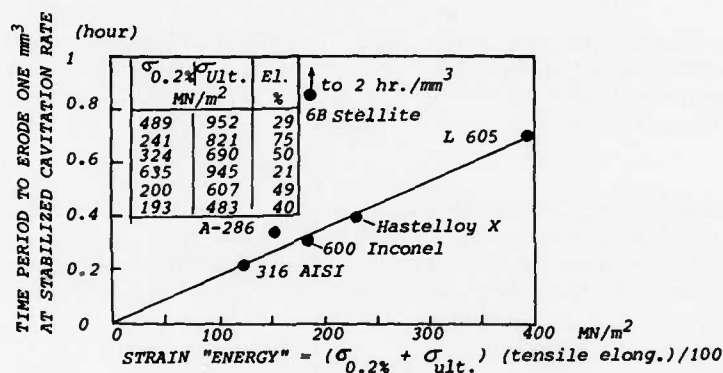
Fig.91   Correlation of the time for unit cavitation erosion in liquid sodium at 427°C
with the strain energy as defined by Young and Johnston[269]

$\frac{mm^3}{hour}$

6B STELLITE
(Co-30% Cr)
in sodium at 427 °C

PRESSURE
(atmosphere)

4

2.7

Stabilized
erosion rates

1

0   240   480 min.
EXPOSURE DURATION t
(a)

$\frac{mm^3}{hour}$

L-605

PRESSURE
(atm.)   4

3

2
1

0   120   240 min.
EXPOSURE DURATION t
(b)

$\frac{mm^3}{hour}$

316 AISI STEEL

Stabilized
erosion rate

PRESSURE
4

2.7

1

0   120   240 min.
EXPOSURE DURATION t
(c)

Fig.92   Influence of static pressure on cavitation erosion rate, Ade_m/dt, in liquid sodium at 427°C,
of specimens subjected to magneto-striction vibrations of 44.5 μm-amplitude at a frequency of 25 kHz,
from Young and Johnston[270]

In logarithmic coordinates the straight lines in Figure 93 make it possible to interpolate the pressure/corrected erosion rate relationship, while the level curves in Figure 94, marked as erosion rates, permit an interpolation to show the effect of temperature and pressure.
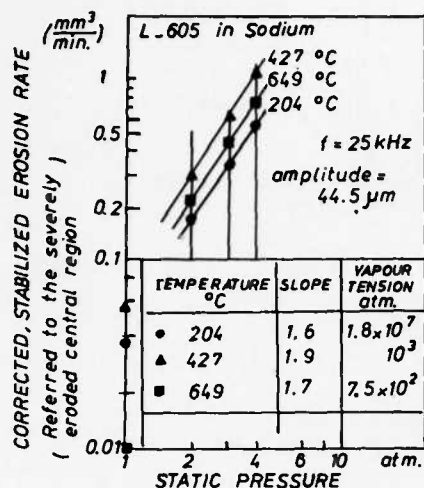
Fig.93 Stabilised erosion rate, corrected for the severely eroded central area as a function of the pressure at temperatures of 427°C, 649°C and 204°C in liquid sodium[270]
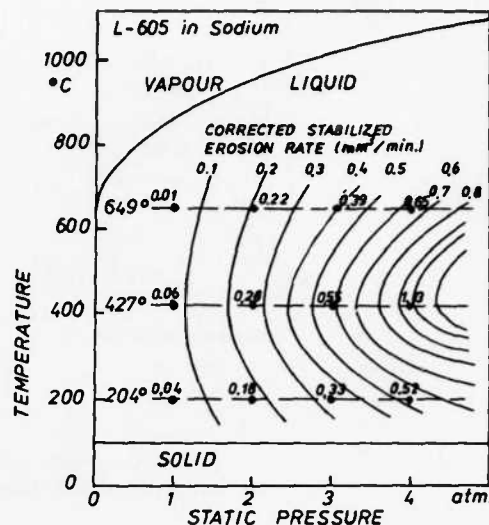
Fig.94 Distribution of the corrected stabilised erosion rate within the pressure-temperature domain for cavitation in liquid sodium. From Young and Johnston[270]

Garcia, Hammitt and Nystrom[271] collated their results of cavitation erosion tests on different metals and alloys in water and mercury at 21°C (Ref.272), mercury and a Pb-Bi 70-30 alloy at 260°C (Ref.273), and the Pb-Bi alloy at 816°C (Ref.274). These tests were performed in a piezoelectric 150 W oscillator at ultrasonic frequency, the cylindrical specimens being screwed on to the end of the oscillator horn. Table 7.5.2.3 − 5a details the properties of the fluids used as cavitation baths.

TABLE 7.5.2.3 − 5a

Physical Properties of Fluids used in Cavitation Tests carried out by Garcia et al.[271]

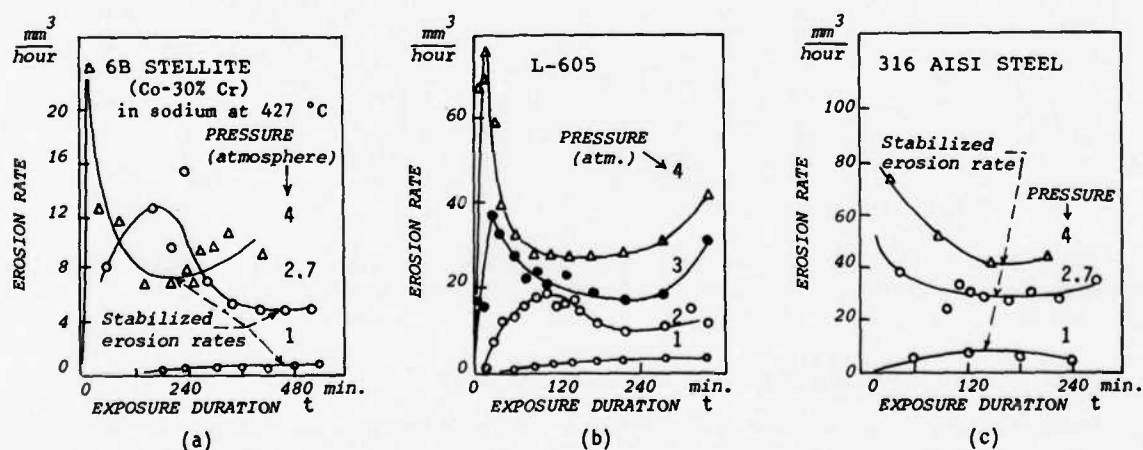| Properties	Units	Water, 21°C	Mercury, 21°C	Mercury, 260°C	Pb-Bi, 260°C	Pb-Bi, 1500°C
Acoustical impedance ($c\rho$),	$g/cm^2 s$	1.46×10^{-5}	1.97×10^{-5}	1.88×10^{-5}	1.505×10^{-5}	1.34×10^{-5}
Density , ρ	g/cm^3	1	13.55	12.98	10.38	9.64
Surface tension,	dyne/cm	72.8	465	419	397	367
Suction height,	m	11.13	0.823	0.854	1.0675	1.159
Bulk elastic modulus,	MN/m^2	2139	28359	27186	21800	20150
Cinematic viscosity,	cm^2/s	0.01	0.0011	0.00077	0.00165	0.0012
Thermal conductibility,	$cal/s\ cm°C$	1.41×10^{-3}	0.021	0.030	0.025	
Vaporization heat,	cal/g	585	69.7	69.7		
Vapour pressure at 21°C	N/m^2	0.0025	0	0.0133	0	0

c is the sound velocity within the liquid.

The results of these tests are contained in Figures 95(a) and 95(b) and in Table 7.5.2.3 − 5c, showing the mean rates of penetration in depth, de_m/dt in $\mu m/h$, for the region of the linear relationship between e_m and t, that is, the maximum values.

7.5.2.3 − c − Cavitation in lubricating systems and hydraulic equipment

Problems relating to cavitation in lubricating systems of machines and in hydraulic equipment for transmitting force or movement have been reviewed by Hobbs and McCloy[275]. Cavitation bubbles may originate from the gases dissolved in the liquid if the pressure falls below the saturation pressure, or from vaporization of the liquid at a lower pressure which is less than the vapour tension.

The solubility of a gas in a liquid is proportional to the pressure. For example[275], mineral oils dissolve per atmosphere of pressure a 10% volume of air considered to be at 21°C and a pressure of 1 atm. If the liquid is saturated

TABLE 7.5.2.3 – 5b

Mechanical Properties of Materials Tested in Cavitation by Garcia et al.[271]

Materials	$\sigma_{ult.}$ MN/m^2	$\sigma_{0.2\%}$	[†] $\int\sigma\varepsilon d\varepsilon$	True strain energy [††] MN/m^2		DPH [†††] Hardness	Ductility Elong.%	ar.red Σ%	Modulus E, MN/m^2
Tests at 21°C									
304 austenitic stainless steel (19%Cr, 10%Ni)	652	446	395	285	328	237	63.8	77.9	200000
316 austenitic Stainless steel (18%Cr,13%Ni,Mo)	602	439	337	264	342	227	57.8	80.3	200000
T-111 Tantalum alloy	908	862	116	110.4	473	308	14.8	80.4	193000
T-222 Tantalum alloy	1064	1063	105	111	485	338	10.6	55.6	193000
do., annealed	751	629	165	153	361	288	23.1	61.1	193000
Molybdenum, 0.5% Ti	1144	1038	147	101	80	295	9.3	7.9	310500
Columbium, 1% Zr.	408	407	46	43	204	151	14.3	88.4	103500
do. annealed	250	132	91	7.2	12.1	99	41.9	91.4	103500
Tests at 260°C									
304 stainless steel	638	391	111.4	125.5	257	154	30.8	72.9	179400
316 stainless steel	500	361	125	122	262	203	30.4	78.2	179400
T-111 Tantalum alloy	702	695	104	74	351	218	13.8	86.2	186300
T-222 Tantalum alloy	923	923	88.7	89	468	286	10.9	71.5	186300
do. snnealed	637	437	142.4	233	291	209	23.6	66.9	186300
Molybdenum, 0.5% Ti	580	550	73.8	75.9	306.4	207	15	75.9	296700
Columbium, 1% Zr	377	377	44.5	35.8	191	133	12.7	88.7	100000
do. annealed	172.5	80	56	26	54.4	71	35.9	92.2	100000

(†) $\int\sigma\varepsilon d\varepsilon$ is the "strain energy" computed from the engineering static stress-strain curve, $\sigma_{nominal} - \varepsilon_{apparent}$,

(††) Two values of the "true strain" are used. The first value ascribes the true strain, computed from the reduction in area of the cross section Σ, to the whole specimen length; the second value takes account of necking by computing the local ε.

(†††) Diamond Pyramid Hardness.
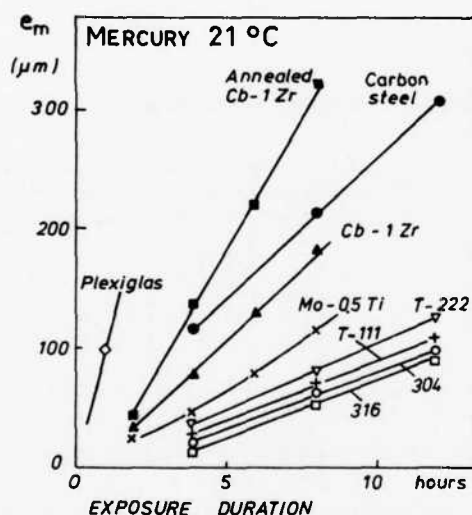
Fig.95(a)   Cavitation erosion in mercury at 21°C pressure = 1 atm., ultrasonic frequency, from Garcia et al.[271]
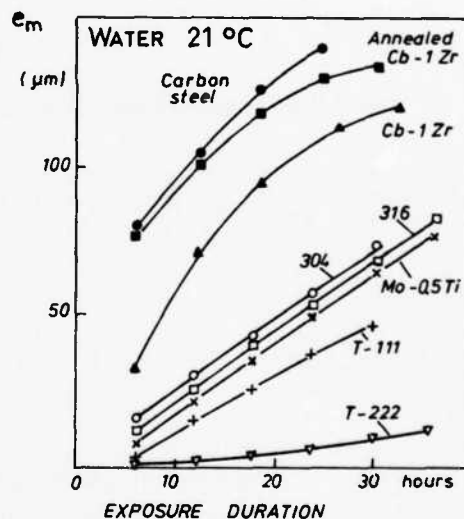
Fig.95(b)   Cavitation erosion in water at 21°C, pressure = 1 atm., ultrasonic frequency[271]

with dissolved air in a tank in which it is in contact with the air, and is then subjected in turn, because of the flow, to a lowering of the pressure caused by suction of a pump, to pressure increases in front of the flow barriers and reductions behind these barriers, gas bubbles form during the low pressure periods and collapse when the pressure rises again.

At low pressures which are below the vapour tension of the liquid, vapour forms on the free surfaces of the liquid and, within the liquid, on the surface of the gas bubbles imprisoned in the roughnesses or cracks on the surface of the mechanical components.

Pressure variations are encountered wherever there is a fluid flow or vibration from a wall, in particular:

Fig.95(c)   Cavitation erosion in mercury at 260°C
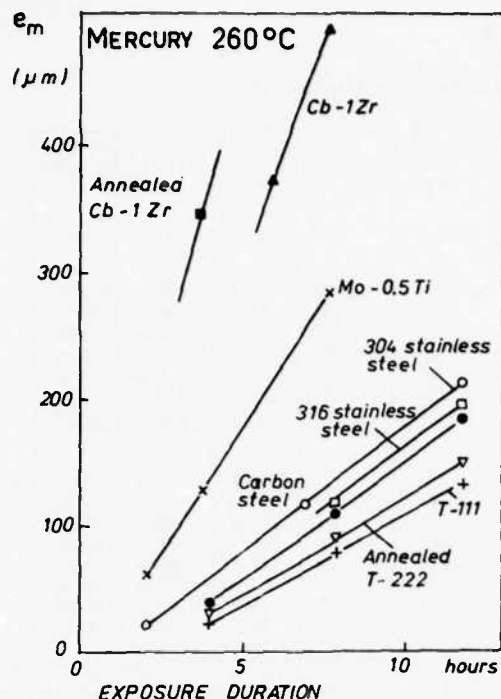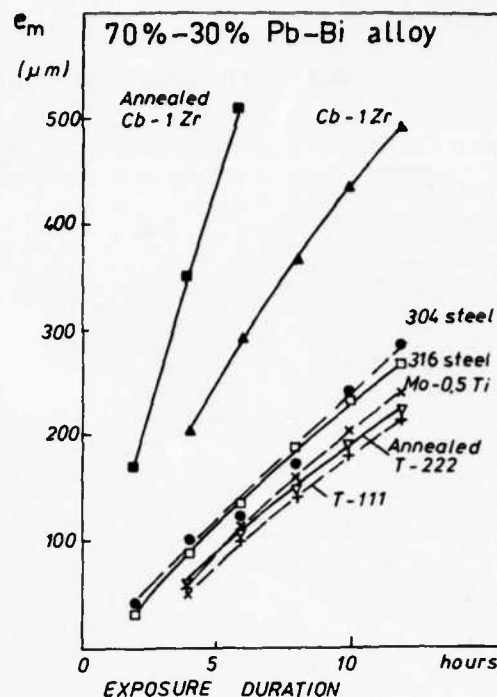pressure = 1 atm., ultrasonic frequency[271]

Fig.95(d)   Cavitation erosion in the melted
70-30 Pb-Bi alloy at 260°C, pressure = 1 atm.,
ultrasonic frequency[271]

TABLE 7.5.2.3 — 5c

Values of the Stabilised Erosion Rate, $(de_m/dt)_{max}$ in Cavitation Tests with Various Liquids, from Garcia et al.[271]

Bath and temperature	Stainless steels		Tantalum alloys			Mo-$\frac{1}{2}$Ti	Cb-1Zr	anneald Cb-1Zr	Carbon steel	2024 T351	6051 T651	Plexiglas	Aluminium 1100-0
	304	316	T-111	T-222	annealed T-222								
Water 21°C	2.5	2.3	1.5	0.5		2.3	3.8	4.6	5.8	14.5	18.3	1390	2700
Mercury 21°C	8.2	8.4	8.9	10.9		14.5	23.4	40.9	26.2			101	
Mercury 260°C	17.5	11.7	10.9		11.7	27.7	61.7	94.7	15.5				
Pb-Bi 260°C	22.4	19.8	18.3		19.3	19.8	41.4	90					
Pb-Bi 816°C	287	71.1	21.3		22.4	27.4	55.6	96.5					

— in the turbulent region of the fluid flow, e.g. after passing through an immersed hole, or through an annular gap in a flowrate or pressure regulating device, tap, valve or slide valve;

— in the turbulent boundary layer of the flow at the wall of tubing comprising changes of direction or roughnesses;

— in the case of fluid flow along a wall excited by high frequency vibrations, as in the cavitation of cooling jackets in internal combustion engines, or of the plain bearings in these engines.

The usual type of high frequency cavitation tests involves a moving immersed specimen which is caused to vibrate in a piezo-electric or magneto-strictive device, or a fixed immersed specimen which undergoes pressure variations induced by a similar fixed specimen screwed on to the vibrating device at a short distance from the first-mentioned fixed specimen. This arrangement has the advantage that the inertia of the specimen is no longer a limitation. There is, however, the disadvantage that the quantity of gas dissolved in the fluid cannot be checked separately from the fluid pressure. To meet this requirement Hobbs and Rachman[276] used apparatus, shown in Figure 96, which made it possible to measure the temperature and the pressure of the pulsed fluid film between a fixed and a moving specimen.

The fluid film is continually being renewed; there is no parasitic mechanical stressing of the specimen and two different materials can be used to simulate electrolytic effects of contact. The apparatus is very suitable for tests on oils, anti-friction metals and plastic metal coatings.
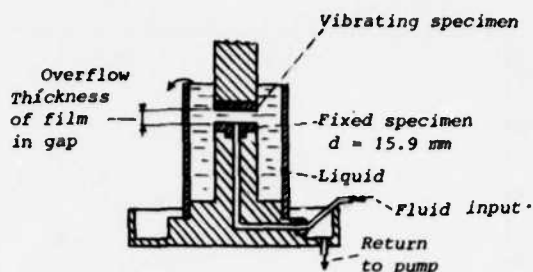
Fig.96   Magneto-striction oscillator, frequency = 20 kHz,
amplitude = 50 μm

The static pressure, measured through orifices with an outlet at the surface of the lower fixed specimen, varies from a pressure drop in the centre to an overpressure which falls to zero, at the edge. The radial static pressure distribution is shown in Figures 97(a) and 97(b) for two different widths of the gap and various values for the water flowrate. The unit of pressure has not been stated.

As illustrated in Figure 98, the temperature rises fairly rapidly from the centre and varies only slightly thereafter. The mean temperature rise depends on the fluid and its flowrate.
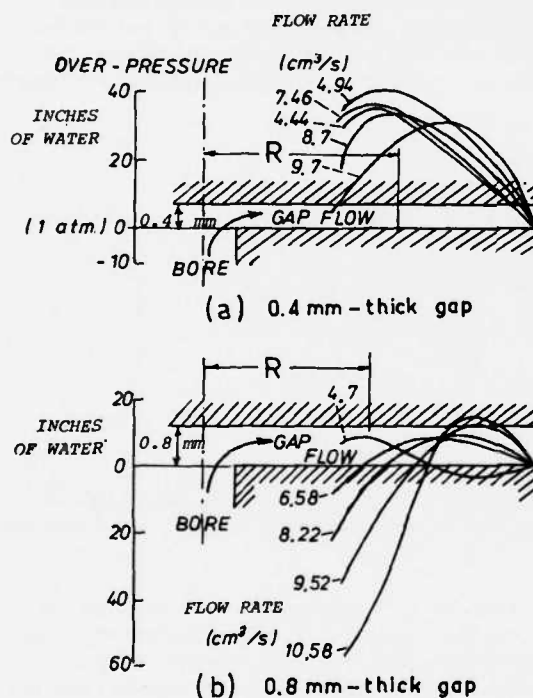
Fig.97   Radial pressure distribution in cavitation
tests with central water supply,
from Hobbs and Rachman[276]
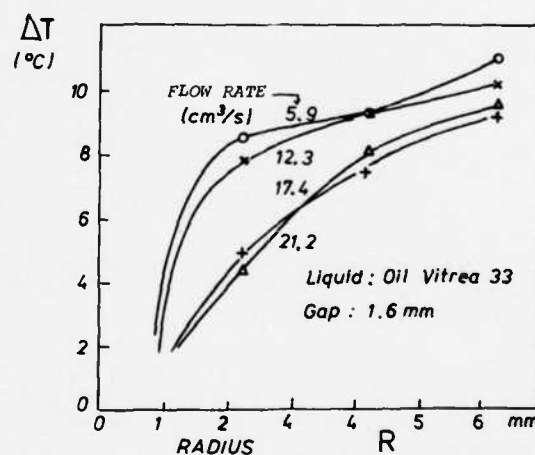
Fig.98   Temperature rise due to the
vibration energy[276]

The authors investigated the behaviour of a tin based anti-friction coating (90% Sn, 7% Sb, 3% Cu) deposited on a steel bearer, for coating thicknesses of 0.075, 0.2, 0.25 and 0.46 mm. The erosion losses in mg are shown in Figure 99 as a function of time and the thickness of the coating. The 0.46 mm thick specimen behaved in the usual way, the erosion rate being lower after a certain time. Examination of the specimens under the microscope showed considerable hardening of the 0.46 mm specimen after 12 minutes; a test conducted on a 1.3 mm specimen suggested that cracks originate at the ends of the Cu_6Sn_5 needles and are propagated along the interfaces with the matrix. Once the cracks have reached the surface of the bearer metal, the material begins to peel, which explains why the specimens with a thin coating did not reach the steady cavitation erosion rate.
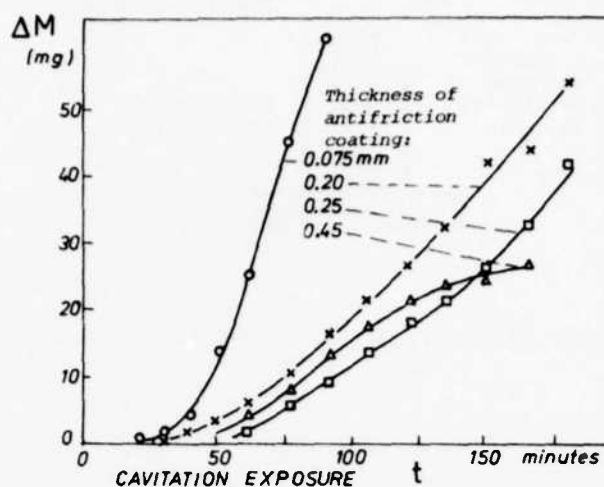
Fig.99   Mass loss of an anti-friction coating on a steel bearing due to
cavitation within an oil film, from Hobbs and Rachman[276]

Kosirev[277] investigated oil drop impact erosion using oils of varying viscosity and a rotating arm carrying steel specimens which hit a jet of oil perpendicular to the plane of rotation at impact velocities of between 40 and 100 m/s. Erosion decreased with increased viscosity, disturbing the lateral flow of the fluid and penetration into the pits. Table 7.5.2.3 − 6 shows the effect of the fluid viscosity on the relative mass loss by erosion, as compared with that produced by water.

TABLE 7.5.2.3 − 6

Relative Mass Losses by Liquid Impact at $V = 60$ m/s, from Kozirev[277]

Fluid	Kinematic viscosity at 30°C ν (cts)	Mass loss M	Relative mass loss M_{Water} / M_{Fluid}
Water	0.18	394	1
Gas-oil	2.6	294	0.746
No. 2 oil (spindle)	27.7	144	0.365
Diesel De-11 oil	185	58	0.147
Automobile oil	381	22	0.055

These fluids are classified in the same order as that relative to the pitting fatigue observed in the fatigue tests on bearings[278]. Tichler and Scott[279] had noted a correlation between cavitation erosion and rolling contact fatigue resistance in the case of ball bearing steels.

In the cavitation tests the pits appear before the deep craters. Tichler et al.[280] investigated chromium steels and came to the conclusion that two periods of uniform erosion could be observed during the process of magneto-striction cavitation erosion at 20 kHz. During the first period, the erosion rate is high and the surface is attacked uniformly, although isolated pits (d ~ 100 μm) form after a certain time. During the second period of a uniform erosion rate, the surface is saturated with deep individual craters (500 to 1000 μm) and the erosion rate is relatively low. In the case of the chromium steels studied, there is a linear relationship between the inverse dt/de_m of the erosion rate during the first period and the true tensile strength σ_R^*.

In a subsequent paper when studying 6 chromium steels and 6 Cu-Ni alloys, Tichler et al.[281] found a correlation, $R_e = A(\sigma_R^*)^n$, with n close to 2.3, between the erosion resistance $R_e = dt/de_m$ and the true tensile rupture stress σ_R^*. The mean erosion depth at the first pit, $(e_m)_p$, was determined for two stellite type cobalt alloys and three steels (case hardening, nitriding and maraging) during cavitation tests at 20 kHz in water at 35°C with a bichromate corrosion inhibitor at a pressure of 1 bar. The test results showed no correlation between $(e_m)_p$ and the erosion resistance $R_e = dt/de_m$ during the first uniform erosion period.

Assuming that the small pits which initiated the craters were formed by surface fatigue, the authors[280] performed tests on two ball bearing steels (A and B in Table 7.5.2.3 − 7) and two high speed cutting steels (C and D). Cavitation erosion was measured by the uniform rate de_m/dt in the first period, and the time before the appearance of the first pit was noted after a continuous visual examination. The erosion resistance values, $R_e = dt/de_m$, were identical for the four steels at 17.4 x 10^{-9} s/m. The Table however shows different values for the mean depth of erosion $(e_m)_p$ at the appearance of the first pits.

TABLE 7.5.2.3 – 7

Comparision of Ball-Bearing Fatigue Life and of Erosion Depth in Cavitation Tests, from Tichler et al.[280]

Material	Ball-bearing fatigue life[279]		Cavitation tests Mean erosion depth at ocurrence of first pit μm
	15,000 r.p.min. load = 600 kg oil lubricated	20,000 r.p.min. load = 280 kg diester lubricated	
A Ball-bearing steels	7.3×10^3 rev. 3.5		57 29
C High-speed cutting steels		23.5×10^3 rev. 13.1	12 1

In each group the steel with the greatest resistance to rolling fatigue also has the greatest resistance to the formation of cavitation pitting.

7.5.2.4 Liquid Impact Erosion of Transparent Materials, Reinforced Plastics and Laminated Materials

Aircraft cockpit canopies and windows are made of glass or plastic materials which are transparent to light. Front canopies are made of layers of glass and plastic materials bonded together. This lamination of thick sheets of material is designed to provide greater resistance to the tensile stresses set up by impact from birds with which aircraft may collide at high speed. To avoid immediate destruction of transparency by liquid impact due to water droplets the outer surface of the front glass sheet is hardened by quenching or by chemical etching.

The windows to be used for infra-red photography are protected by sheets of quartz which are transparent to infra-red radiation. The radomes must be transparent to electromagnetic waves. They are made of glass fibre reinforced plastics giving the complete unit high mechanical strength, and are protected against damage from rain impact by coatings which are more flexible and more erosion resistent.

7.5.2.4 – a – Liquid impact resistance of solid transparent materials

In addition to the ductile metals and alloys investigated above, the materials used in the construction of aircraft and helicopters, and which are subjected to the erosive action of rain and dust are:

— the glasses and various resins, which admit light;

— the lead glasses and quartz, which admit infra-red rays;

— the glass fibre reinforced resins and ceramics, which admit electro-magnetic waves;

— the elastomers.

An early comparison of the behaviour of these materials and that of metals under repeated rain drop impacts can be found in the tests by Behrendt[282] performed with a rotating arm in a chamber with a partial vacuum of 6 to 18 mm Hg at impact velocities of between 400 and 1000 m/s; the rain was produced by oscillating tubes. The life was measured by the cumulative height of the water which fell on the unit area:

$$h = V t \rho_{w/a} ,$$

where $\rho_{w/a}$ is the volume concentration of the water in air. Tests at constant V_{rain}/V_{sound} Mach numbers of 1.4 and 3 were carried out at impact velocities V ranging from 200 to 400 m/s for Mach 1.4 and 300 to 1000 m/s for Mach 3, V and the test pressure being varied.

For the metallic materials the incubation time t_i and the maximum erosion rate $(de_m/dt)_{max}$ vary according to the following expressions (see Equations (99) and (100), as well as Table 7.5.2.2 – 1):

$$t_i = a/V^m , \tag{99}$$

$$(de_m/dt)_{max} = b V^n . \tag{100}$$

Table 7.5.2.4 – 1 gives the values for the exponents m and n for various materials tested by Behrendt.

In addition, Rieger's tests[283], some results of which are contained in Table 7.5.2.4 – 2, show that the exponents m and n vary with the rain drop diameter.

TABLE 7.5.2.4 – 1

Values of the Exponents m and n in Relationships (99) and (100) for the Erosion Incubation Period
and the Erosion Rate as a Function of the Impact Velocity in Behrendt's Rain Erosion Tests[282]
with 1.2 mm Diameter Rain Drops

Material	m-values		n-values	
	V = 400-1000 m/s	V = 250-400 m/s[†]	V = 400-1000 m/s	V = 250-400 m/s[†]
Metal and alloys				
Pure aluminium	2.6	4.9	3.8	2.8
Al Mg Si 1	3.9	4.9	5.3	6.2
Al Cu Mg 2	3.9	5.4	4.8	5
Ti Al 6 Mg 2	4.8		7.4	
Ti (IMI 680)	4.1		6.1	
Plastics				
Polyurethane	4	7.4	13	4.4
Fiber-reinforced plastics	3		3.7	
Transparent acrylic	2.9	3.6	1.9	2.4
Various				
Silicate glass	3.8	5.7	6.1	7
Sapphire (Al_2O_3)	3.4	20	9.5	
Ceramic "Degussit" Al 72	3.4	7.4	7.4	5.6

[†] Values from Rieger[283]

TABLE 7.5.2.4 – 2

Variation of Exponents m and n as a Function of Rain Drop Diameter from Rieger's Tests[283]

	m-values			n-values			
drop diameter, mm	0.5	1.2	1.7	0.5	1.2	1.7	mm
Aluminium	4.4	4.9	3.6	3.6	2.8	4	
High pressure polyurethane	1.4	5.6	8.4	3.8	5.1	7.8	
Polyurethane	6.7	7.4	9	4.3	4.4	4.4	
Polycarbonate (Makrolon)	3.7	4.6	5	3.2	3.7	3.5	
Plexiglas	3	3.6	3.8	2.6	2.4	1.6	
Glass		5.7					
Sapphire (melted Al_2O_3)		7.4					

The impact frequency (per second on 1 cm^2) and the rain drop diameter have little influence on the maximum erosion rate. However, in the case of sapphire and polyurethane the volume of rain required for erosion incubation decreases with increasing frequency. The incubation time is reduced and the maximum erosion rate of high pressure polyurethane increases for an increase in the diameter of the rain droplets.

The expression for the maximum erosion rate as a function of the impact velocity is not suitable for investigating the transparency life of aircraft canopies. According to Schmitt[264], rain erosion damage at subsonic aircraft speeds causes the formation, on the glass, of individual cavities which are likely to become joined together, with subsequent detachment of larger elements. At supersonic speeds[222] catastrophic rupture occurs creating large cracks. At low supersonic speeds all the materials tested lost their transparency (80% transmission loss), even if the material loss was not capable of being measured[285]. The transparent plastic materials investigated were a UV stabilised polycarbonate Lexan 9034 provided by the General Electric Company and a polysulphone Bakelite P-1700 made by the Union Carbide Corporation. These materials, the physical properties of which are given in Table 7.5.2.4 – 3, behave better at high temperatures than the acrylics, are less expensive than the glasses and have good mechanical strength and good optical transmission characteristics. The purpose of the study was to determine the effects of rain at subsonic impact velocities on the transmission of monochromatic radiation with a wavelength of 1.06 μm.

The specimens, held by mountings with angles of 90, 60, 45 and 30° between their surfaces and the impact velocity of the rain droplets, were mounted on a 4340 steel helicopter blade with a speed of 400 m/s at the blade tip under a 2.4 m diameter tubular ring provided with 96 hypodermic needles dispensing rain of 25.4 mm/h with 1.5 to 2 mm diameter droplets. The plane specimens were dried in a stove at 38°C, the weight and optical transmission being measured before and after each erosion stage. In 101 of the 110 specimens the weight increased by 0.1 to 0.2% after erosion, probably due to humidity retention. The results show that erosion does not remove any material, although it affects optical transmission. The surface layers become dull or "frosted" by pitting. The tests were terminated during the incubation period of the erosion process. Table 7.5.2.4 – 4 shows that the transparency losses were negligible after 20 minutes' exposure at normal velocities of less than 155 m/s but that in the case of the polysulphone and the polycarbonate when tested at a normal velocity of between 230 and 270 m/s and at an angle of between 90 and 60°, the transparency dropped respectively to 70% and 20% of the initial values. Similar reductions were observed without loss of weight on lead glass which transmits infra-red, quartz, germanium, calcium aluminate, magnesium fluoride, yttrium oxide Y_2O_3, silica, magnesium oxide and the sapphire single crystal[285]. It may be concluded that the period of incubation of weight loss by erosion is not a correct measure of the damage which occurs in transparent materials.

TABLE 7.5.2.4 – 3

Physical Properties of Transparent Plastics, Lexan 9034 Polycarbonate and P 1700 Bakelite Polysulphone, given by the Supplier, from Schmitt[284]

Physical properties	Lexan 9034	P 1700 Bakelite
Specific mass (kg/dm^3)	1.2	1.24
Tensile strength (MN/m^2)	62.1	70.4
Young modulus (MN/m^2)	2380	2184
Tensile elongation at failure ,%	110	50 – 100
Bending strength (MN/m^2)	932	1063
Bending modulus (MN/m^2)	2346	2690
Shear strength (MN/m^2)	69	
Compressive strength (MN/m^2	86	
Rockwell hardness	M70(R118)	M69(R120)
Izod impact strength at 22°C (ft lb/in.)	16	1.3
Hot-deflection temperature , f = 0.254 mm under 1.8 MN/m^2.	132°C	174°C
Note: These values result from application of the ASTM test standards and have been translated into the International System of Units, except for the Izod impact tests		
Light transmittance at a wave length of 1.06 μm	90.4 %	88.2 %

TABLE 7.5.2.4 – 4

Variation of the Optical Transmittance of the Lexan 9034 and P 1700 Bakelite Transparent Plastics after Rain Exposure, from Schmitt[284]

Orthogonal velocity .p.hr.	m/s	Impact angle degree	Nominal velocity m/s	Exposure duration minutes	Transmittance after 25 hr. of rain exposure† Lexan 9034	Bakelite P 1700
400	178	90	400	5	98.4	94.7
				10	98.2	89.4
				20	99.1	87.4
433	192	60	500	2	99.9	94.7
				5	97.8	89.3
				10	97.1	75.2
				20	93	53.1
424	188	45	600	2	96.9	95.1
				5	97.3	88.7
				10	93.4	82.6
				20	88.1	72.7
500	222	90	500	1	99.8	94.1
				2	98.4	86.2
				5	96.6	77.7
				10	90.7	53.9
				20	74	18.3
519	231	60	600	1	95.7	84
				2	94.8	84
				5	90	64.4
				10	78.7	46.6
				20	65.8	25.4
600	267	90	600	1	89.2	81.7
				2	82.3	58.3
				5	56.6	52.6
300	134	30	600	5	97.3	95.3
				10	97	95.5
				20	95.8	91.5
354	158	45	500	5	96.5	93.7
				10	97.1	94.6
				20	97.2	84.3
346	155	60	400	20	97.4	91.7
230	112	30	500	20	97.9	95.5
† Average from two measurements, excepted for 90°-impacts.						

King[286] has compared the rain erosion behaviour of "Perspex" plastic materials (polymethylmethacrylate) and polypropylene with that of ceramics (Sintox and UL 995) and of metals (pure aluminium, L85 aluminium alloy, BS1433 copper and Cr 130 steel). Tests were performed at the RAE Farnborough up to velocities of 223.5 m/s and at Dornier up to 450 m/s, on a rotating arm with 1.2 mm diameter artificial rain droplets. The results are contained in Table 7.5.2.4 – 5 where the mean erosion depth is defined as

$$e_m = \frac{\Delta M}{\rho A} = \frac{\text{weight loss}}{\text{specific weight} \times \text{area exposed}}$$

and in which $h = Vt \times \rho_{w/a}$ is the cumulative height of the water in rain with a water/air density $\rho_{w/a}$.

TABLE 7.5.2.4 − 5

Rain Erosion Tests, from King[286]

Material	Impact velocity (m/s)	Erosion duration (min.)	Rain density $\rho_{w/a}$ $\frac{cm^3}{cm^3}$	Loss (mg)	Maximum erosion rate (mg/min.)	Mean erosion depth, e_m mm	Average water height h, (cm)
Plastics							
Perspex	450	0.25	2.5×10^{-6}	274	1752	1.3	1.7
	400	0.33	do.	302	1422	1.41	2
	350	0.66	do.	397	1194	1.89	3.5
	300	2	do.	417	307	1.99	9
	250	6	do.	402	81	1.91	22.5
	223.5	12	do.	448	71	2.13	40.2
Polypropylene	450	1.5	2.5×10^{-6}	81	86	0.5	10.1
	400	3	do.	133	52	0.83	18
	350	8	do.	137	24	0.83	42
	300	12	do.	80	13	0.5	10.1
Alumina ceramics							
"Sintox"	450	10	1×10^{-5}	436		0.67	270
	450	15	2.5×10^{-6}	40		0.06	101
	400	15	1×10^{-5}	48		0.07	310
	300	18	1×10^{-5}	1.2		0.002	324
UL 995	450	6	2.5×10^{-5}	230		0.35	40.5
	300	6	1×10^{-5}	3.1		0.005	108
Aluminium, 99.5	450	2	2.5×10^{-6}	244	134	0.51	13.5
	400	3	do.	232	81	0.49	18
	350	7	do.	356	52	0.75	36.8
	300	15	do.	303	21	0.64	67.5
	250	25	do.	140	7	0.29	83.8
L85 Al alloy	450	7	2.5×10^{-6}	256	42	0.53	47.3
	400	15	do.	289	23	0.60	90
	350	40	do.	309	11	0.64	210
BS 1433 Copper	450	6	2.5×10^{-6}	589	114	0.37	40.5
	400	10	do.	536	74	0.36	60
	350	20	do.	573	39	0.34	105
	300	45	do.	439	17	0.28	202.5
CR 130 steel	450	15	1×10^{-5}	647	71	0.47	405
	400	35	do.	414	38	0.30	840

Table 7.5.2.4 − 6 below, by the same author, compares the theoretical impact velocity thresholds for the damage, calculated by means of the erosion rate $d\Delta M/dt$, such that

$$d\Delta M/dt = k(V - V_i)^m , \tag{106}$$

where ΔM is the weight loss and V_i is the velocity threshold lying at the intersection of the tangent to the $\Delta M(V)$ curve with the axis of the impact velocities V.

TABLE 7.5.2.4 − 6

Computed Values of the Threshold Velocity V_i for Rain Erosion Damage and of Equation (105)'s Constants, from King[286]

Material	V_i (m/s)	m	k
Polymethylmethacrylate (Perspex	90	3.23	9.70×10^{-6}
Polypropylene	113	2.92	4.28 "
Aluminium (99.5 %)	127	3	3.98 "
L 85 aluminium alloy	148	3.32	2.46 "
BS 1433 Copper	140	3.04	3.37 "

Although a rough qualitative classification of the various materials can be deduced from the above Tables by using the materials common to several Tables to make such classifications, a comparison depends too much on the circumstances peculiar to each type of specimen test to give more than a preliminary indication which would have to be supplemented by more representative tests of the structure under consideration before a final direct verification in service conditions could demonstrate the actual value of the comparison.

7.5.2.4 − b − Laminated materials and coatings

Schmitt[222] has provided a set of erosion test results for specimens carried by planes inclined at varying degrees θ to a wedge-shaped sled propelled on rails by rockets over a length of 1818 m equipped with nozzles which provide simulated

natural rain (Holloman Track Test Facility). Getting up to speed was effected over a track length of 2424 m, while after braking over a distance of 6514 m through polyethylene foam, the specimens could be dismantled, inspected and weighed.

The mean penetration depth rate in the direction of the impact velocity, de_m/dt, is proportional to $(V \sin \theta)^n$ and the number of droplets encountered, is proportional to $V \sin \theta$, while the depth of penetration along the perpendicular to the surface is

$$(de_m/dt) \sin \theta = K (V \sin \theta)^p \tag{107}$$

where $p = n + 1$.

Table 7.5.2.4 – 7 gives the values for p and K, together with the coefficient of correlation r for the tests on various transparent materials and various plastics.

TABLE 7.5.2.4 – 7

Comparative Tests of Simulated Rain Erosion on the Running Wedge of the Holloman Track Test Facility, from Schmitt[222]

Material	p	K	Correlation r
753 Alumina	9.476	5.41×10^{-35}	0.856
754 Beryl	4.272	2.81×10^{-17}	0.678
9606 Pyroceram	6.549	8.39×10^{-24}	0.874
701 Cordierite	10.128	1.29×10^{-35}	0.815
7941 fused silica	5.422	1.11×10^{-19}	0.888
Furane 8 265 epoxy laminate	6.414	1.06×10^{-23}	0.981
Epon 828 epoxy laminate	6.548	5.01×10^{-24}	0.940
Shygard 700 polyimide laminate	6.522	1.13×10^{-23}	0.888
Polybenzimidazole laminate	5.430	8.28×10^{-20}	0.985
Aluminium phosphate laminate	5.214	7.71×10^{-19}	0.919
0.254 mm neoprene/epoxy laminate	7.034	2.37×10^{-20}	0.900
0.91 mm Rokide A aluminium/epoxy laminate	6.928	7.79×10^{-30}	0.962
C 106 Cer-Vit glass-ceramic	8.34	9.62×10^{-29}	0.887
9753 infrared glass	6.59	2.88×10^{-23}	0.861
7913 windshield glass	5.84	1.98×10^{-20}	0.760
1723 glass	9	4.4×10^{-31}	0.921
Polyphenylene oxide	6.88	1.25×10^{-25}	0.860
Plexiglas	6.55	3.83×10^{-24}	0.982
Teflon	5.067	8.26×10^{-19}	0.965
Polycarbonate	7.73	3.19×10^{-28}	0.938
A-1100 aluminium	7.27	5.12×10^{-28}	0.948

In this type of test at supersonic speeds, the aerodynamic flow is disturbed by the shock waves emitted from the various edges of the running wedge and the specimens. It is possible, however, to establish a preliminary comparison of the behaviour of the different materials which will help to narrow the field of investigation in subsequent tests on more extensive and more representative structures than the small specimens.

At hypersonic speeds, up to 1700 m/s, the speed component tangential to the surface assumes increasing importance and Schmitt et al.[221], when repeating the running wedge tests with ceramics, laminated plastics and composite materials, reflected the results of these tests in another expression:

$$de_m/dt = K V^p \sin^2 \theta \tag{108}$$

where K and p are given in Table 7.5.2.4 – 8. The statistic of the number of water droplets of a mean diameter equal to or greater than d mm per m^3 of air in the simulated rain in these tests and in those covered by Table 7.5.2.4 –7 has been determined by the measurements carried out by Mueller and Sims[287] and can be represented by:

$$\log_{10} N \approx 3.55 - 0.91 \, d. \tag{109}$$

These results show the range of the field of values for weight loss by erosion in simulation tests on specimens. However, as noted more recently by Schmitt[284], the mean erosion rate is a secondary characteristic for transparent materials as compared with the resistance to impact by birds and the preservation of transparency in erosion conditions affecting transparency, before weight losses become great enough to be capable of measurement.

7.5.2.4 – c – Transmission of pressure and stress waves in laminates – Attenuation by coatings

Certain fibre reinforced plastics are very resistant to mechanical stresses applied in the tangential plane of thin structures but become rapidly damaged by the normal impact of dust and rain. Such impact tends to separate the resin bonded fibres, which have a relatively low cleavage strength. Protective coatings are therefore essential.

TABLE 7.5.2.4 − 8

Rain Erosion Tests Using the Running Wedge at 1700 m/s-Velocity on Ceramics, Plastic Laminate and Composites, from Schmitt et al.[221]

Material	p	K	Correlation r	Test number
Ceramics				
7941 fused silica	4.48	9.22×10^{-17}	0.797	36
Pyrolytic isotropous Boron nitride	4.64	6.05×10^{-17}	0.902	28
Silicon carbide (0.51 mm grains in a graphite matrix)	5.24	1.11×10^{-19}	0.910	29
Plastic laminate and composites				
Glass-epoxy B265 Furane	6.53	1.32×10^{-24}	0.981	32
Glass-epoxy 828 Epon	7.57	3.49×10^{-28}	0.970	41
Glass-polyphenylene oxide (531-801)	5.76	8.9×10^{-22}	0.958	35
Glass-polyimide compact	6.25	7.8×10^{-24}	0.956	25
Glass-epoxy composite	4.8	1.28×10^{-18}	0.863	19
Polyphelnylene oxide 531-801 compact	8.72	9.80×10^{-33}	0.983	29
Plexiglas (type II-UVA	6.4	5.54×10^{-24}	0.959	28
Trifluorethylene resin TFE	4.64	1.13×10^{-17}	0.978	55

Hammitt et al.[226] investigated the behaviour of various elastomers when subjected to impact by discontinuous liquid jets 1.2 mm in diameter, at a velocity of 223 m/s and a frequency of 30 jets a minute. The jets were triggered when a steel hammer struck a diaphragm in contact with a small quantity of water shutting off the rear portion of a cavity comprising a calibrated orifice (see Figure 68, paragraph 7.5.2.1 − a). In the gun tests the incubation period increased and the weight loss decreased for an increasing Shore hardness, from natural rubber with a Shore hardness of 36, to an elastomer with a Shore hardness of 75–80, via several neoprenes.

Calculations of the transmission and reflection of shock waves due to liquid drop impact on the coating and through one or more substrate layers were presented at the same time, at the 4th International Conference in Meersburg on rain erosion and related phenomena, by Springer et al.[288], Engel[289] and Rieger and Roche[290]. The three papers presented assumed that the stress waves being propagated through the coating and the substrate were plane waves, although the pressure due to liquid drop impact was in fact being propagated radially. All the calculations were made on the assumption of the linear elasticity of the materials, although the viscosity of the plastic materials and the plasticity of ductile metals may be factors in actual conditions. It was again assumed that the liquid droplet and the surface of the coating remained in contact for a long time compared with the multiple reflections of the stresses, although this phenomenon is attenuated before another droplet hits the surface at the same point. No account is taken of any lateral dissipation of energy by shearing between the layers, radial attenuation, viscosity etc.

Springer et al.[288] considered merely the case of the coating and a substrate. The calculations made, like those of Engel[202d] (see paragraph 7.5.1.2 − a), correspond to the axial impact of two bars of different material, one representing the liquid droplet and the other the substrate but with a thin layer of coating in between. $c = \sqrt{(E/\rho)}$ is the speed of propagation of a shock wave; c_L is for the liquid, c_C for the coating and c_S for the substrate. In the case of a single resistant material the impact pressure of a droplet on the coating is given by Equation (93), becoming in this case:

$$p = \frac{(\rho_L c_L \rho_C c_C)}{(\rho_L c_L + \rho_L c_C)} V. \tag{110}$$

In the case of a material which has one or more layers of a thin coating negligible thickness h_i compared with the thickness of the liquid droplet and the substrate, which amounts to neglecting the delayed return of the waves reflected at the front surface of the liquid droplet and at the rear surface of the substrate, it is possible to calculate the stresses due to successive transmission and reflection through and over the interfaces.

The initial wave on the coating surface hit by the liquid is a hydrostatic compression wave

$$\sigma_1 = p.$$

Assuming once more the reasoning used above in 7.5.1.2 − a for a solid sphere impact, we obtain, in the case of plane waves, on the assumption of propagation in a bar of constant cross-section:

− Direct transmitted wave σ_1:

maintenance of the momentum values during the time Δt:

$$c_L \Delta t \rho_L V_1 = (c_L \Delta t \rho_L + c_C \Delta t \rho_L) V_{1C}$$

and

$$V_{1C} = \frac{c_L \rho_L}{c_L \rho_L + c_C \rho_C} V_1.$$

then, noting $z = c\rho$ the acoustic impedance,

$$V_{1C} = \left(\frac{z_L}{z_L + z_C}\right) V_1 ;$$

shortening of the bar in the sections (see Figure 100); at the left end:

$$\epsilon_1 + (V_1 - V_{1C}) \Delta t/c_L \Delta t = \{z_C/(z_L + z_C)\} V_1/c_L ;$$

but the modulus of elasticity is $E_L = c_L \rho_L^2$ and the stress transmitted is

$$\sigma_1 = E_L \epsilon_1 = \frac{z_L z_C}{(z_L + z_C)} V_1 .$$

— Reflected wave $\sigma_{1R} = \sigma_2 - \sigma_1$ and transmitted wave σ_2:
momentum:

$$z_L V_1 = (z_C - z_L) V_{1C} = (z_C + z_S) V_{2C}$$

and, with the value of V_{1C}, we get:

$$V_{2C} = \frac{2 z_C z_L}{(z_L + z_C)(z_C + z_S)} V_1 ,$$

then, taking into consideration the shortening of the bar in the coating section, the stresses are:

$$\sigma_{1R} = E_C \epsilon_{1R} = c_C^2 \rho_C (V_{1C} - V_{2C}) = V_1 z_L z_C (z_S - z_C)/(z_L + z_C)(z_C + z_S) = \sigma_1 (z_S - z_C)/(z_C + z_S) ,$$

$$\sigma_2 = \sigma_1 + \sigma_{1R} = \sigma_1 (2 z_S)/(z_C + z_S) .$$

Considering the initial stress wave σ_i which hits the interface between the initial environment and the final environment, the stress σ_{iR} reflected by the interface towards the initial material and the stress σ_T transmitted to the final material, we can, as Engel[289] did, generalise the above formulae as follows:

$$\sigma_T = 2\sigma_i z_f/(z_f + z_i) , \qquad \sigma_{iR} = \sigma_i (z_f - z_i)/(z_i + z_f) . \tag{111}$$
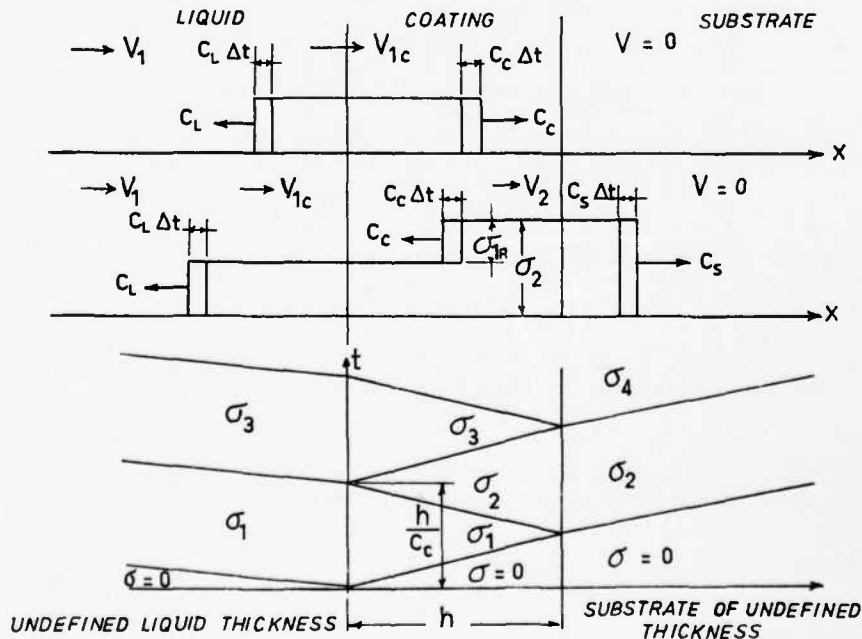

Fig.100   Diagram of stress waves transmitted or reflected during a liquid drop impact on to a substrate covered with a thin coating, from Springer et al.[288]

Continuing the calculations for the successive reflections on the coating/substrate and liquid/coating interfaces, Springer et al. obtained the following expressions

$$\frac{\sigma_{2k}}{\sigma_1} = \frac{1 + \psi_{SC}}{1 - \psi_{SC}\psi_{LC}} [1 - (\psi_{SC}\psi_{LC})^k] \quad \text{with} \quad \psi_{SC} = \frac{z_S - z_C}{z_S + z_C} \tag{112}$$

$$\frac{\sigma_{2k-1}}{\sigma_1} = \frac{\sigma_{2k}}{\sigma_1} - \psi_{SC}(\psi_{SC}\psi_{LC})^{(k-1)} \qquad \psi_{LC} = \frac{z_L - z_C}{z_L + z_C}$$

in which $z = \rho c$ is the acoustic impedance of each material.

The history of the stresses in the coating depends on the relative magnitudes of the acoustic impedance z_L, z_C and z_S. After a large number of reflections, the theoretical stress in the coating at each of the interfaces approaches the common value

$$\sigma_\infty = \sigma_1 \lim_{k \to \infty} \sigma_{2k} = \sigma_1 \frac{1 + \psi_{SC}}{1 - \psi_{SC}\psi_{LC}} = \frac{1 + z_L/z_C}{1 + z_L/z_S} \sigma_1 = \frac{z_S \cdot z_L}{z_L + z_C} V_1 , \tag{113}$$

that is, the stress in the substrate in the absence of a coating.

In view of the numerous causes of damping not taken into account in these calculations, achieving the theroetical limit can be considered as something to be neglected; it is therefore important that the values close to the start of the series should be as low as possible and, in particular, that the stresses σ_1 in the coating and σ_2 in the substrate should be low as compared with σ_∞. According to the results of Springer's calculations shown in Figure 101, this condition is fulfilled by a coating with an acoustic impedance z_C which is less than that of the liquid and the substrate.
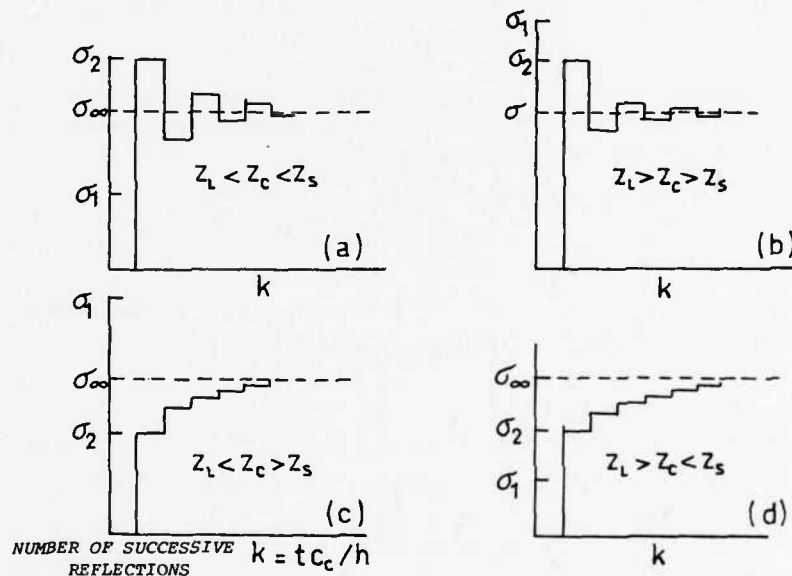
Fig.101   Pressure reduction or rise in the substrate by successive transmissions and reflections of pressure waves through the coating layer, from calculations of Springer et al.[288]

Engel[289] presented similar calculations for a composite coating which included an undercoat. The stress in the wave transmitted to the coating being σ_1, the stress in the wave transmitted to the undercoat will be:

$$\sigma_{T,CU} = \frac{2z_U}{z_C + z_U} \sigma_1 .$$

The stress transmitted from the undercoat to the substrate will be:

$$\sigma_{T,US} = \sigma_{T,CU} \cdot 4z_S z_U \frac{z_S + z_U}{z_U + z_C} \sigma_1 .$$

The stress of the wave reflected by the coating from the coating/undercoat interface is:

$$\sigma_{R,UC} = \frac{z_U - z_C}{z_U + z_C}\, \sigma_1\ .$$

This wave will again be partially reflected in the coating by the liquid/coating interface and the reflected wave will be:

$$\sigma_{R,LC} = \frac{z_L - z_C}{z_L + z_C}\, \sigma_{R,UC}\ .$$

Applying the expressions (111), the numerical calculation can be continued on a computer.

Engel carried out pressure measurements on a coated piezo .:ectric gauge. He considered the various cases: a single soft or hard 0.38 mm thick layer; two layers comprising a hard 0.23 mm thick layer on the surface and a soft 0.15 mm thick undercoat; then the reverse with a soft 0.23 mm surface layer and a hard 0.15 mm thick undercoat. The tests showed excellent behaviour for the hard coating with a single layer and for the double layer coating, the hardest and the thickest layer being at the surface; in these cases the pressures and the rate of loading in the gauge were relatively low. The relative pressure values measured in the four cases showed ratios similar to those of the values calculated by the plane wave theory. It should be noted that the arrival in the substrate of the waves which had undergone various multiple reflections occurred at different times, which may contribute to attenauation.

Rieger and Boche[290] tried to define the shear stresses between the coating layer and the substrate. The following assumptions were made:

(1) The strains are elastic.
(2) The liquid flow lateral jets have no effect during drop impact.
(3) There is only a single reflection at each interface.
(4) The diameter of the virtual bar is assumed to be equal to that of the droplet (plane waves).

Figure 102 shows the notation for calculating the stresses and strains.
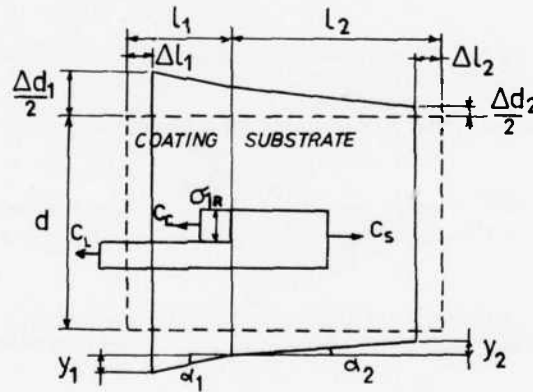
Fig.102   Stress and strain notation used by Rieger and Boche[290] in calculation
of the shear between coating and substrate during rain impacts

For a two layer coating the pressure wave $\sigma_1 = V_1 z_L z_C/(z_L + z_C)$ reaching the surface gives rise to a reflected wave

$$\sigma_{1R} = \frac{z_S - z_C}{z_S + z_C}\, V_1$$

and to a wave transmitted to the substrate

$$\sigma_2 = 2V_1 z_L z_C z_S/(z_L + z_C)(z_C + z_S)\ .$$

The surface layer undergoes compression in the direction of the impact and transverse expansion. Lateral expansion involves subsurface shear. If there is insufficient adherence, separation under shearing τ_s will occur.

Shortening is as follows:

$$- \text{ layer I} \qquad \epsilon_{x1} = \Delta l_1 / l_1 = \sigma_2 / E_1$$
$$- \text{ layer II} \qquad \epsilon_{x2} = \sigma_2 / E_2 \ .$$

Transverse expansion is such that $\epsilon_x / \epsilon_y = \nu$, whence:

with
$$\epsilon_y = \Delta d / d: \ \Delta d_1 = \nu_1 d \cdot \sigma_2 / E_1 \quad \text{and} \quad \Delta d_2 = \Delta d \cdot \sigma_2 / E_2 \ .$$

The adherence condition requires:

$$\tfrac{1}{2}(\Delta d_1 - \Delta d_2) = y_1 + y_2 \ .$$

In addition,

$$y_1 = x_1 \frac{\tau_s}{G_1} = (l_1 - \Delta l_1) \frac{\tau_s}{G_1} = \frac{l_1}{G_1}\left(1 - \frac{\sigma_2}{E_1}\right)\tau_s \ ,$$

$$y_2 = x_2 \frac{\tau_s}{G_2} = (l_2 - \Delta l_2) \frac{\tau_s}{G_2} = \frac{l_2}{G_2}\left(1 - \frac{\sigma_2}{E_2}\right)\tau_s \ .$$

We finally get:

$$\tau_s = \sigma_2 \cdot \frac{d}{2} \cdot \frac{G_1 G_2}{E_1 E_2} \cdot \frac{[\nu_1 E_2 - \nu_2 E_1]}{[l_1 G_2(1 - \sigma_2/E_1) + l_2 G_2(1 - \sigma_2/E_2)]} \ ,$$

where $\nu_1, \nu_2, E_1, E_2, G_1$ and G_2 are respectively Poisson's coefficients, Young's modulus and Coulomb's moduli for the coating and the substrate; d is the diameter of the rain droplet and σ_2 is the pressure in the substrate and in the coating after reflection on the coating/substrate interface.

The following points were observed in the erosion of bonded laminated materials:

(a) Erosion without separation of the coating layers: this applies to glass fibre reinforced resins with a fluocarbon coating.

(b) Detachment of the coating without appreciable erosion: applies to glass fibre reinforced resin specimens which have a polyurethane coating.

In the first case, the strength of the material is determined by the erosion of the coating. Separation frequently occurs in the erosion of laminated plastics.

For coatings consisting of multiple layers of varnish, the conditions of manufacture, such as temperature, air humidity, thickness of each layer, and duration of the drying period between each layer, affect the adherence between the individual layers.

Because of the simplification introduced into the theory, the shear τ_s is merely a comparison parameter. τ_s increases linearly with the droplet diameter and with the velocity V_1 of the impact; its value tends to decrease with an increase in the thickness.

Good results have been obtained with a carbon fibre reinforced resin and a multi-layer polyurethane coating, the rigidity of each layer increasing from the inside to the outside.

Table 7.5.2.4 − 9 shows the rain erosion protection systems investigated by Rieger and Boche.

TABLE 7.5.2.4 − 9

Rain Erosion Protection Systems from Rieger and Boche[290]

Bonded systems	Examples	Applications
Plastic / plastic	Polyurethane / Glass fiber reinforced plastics (GFRP)	Protection of radomes
Metal / plastic	Titanium / GFRP	Leading edges of helicopter blades
	Steel / GFRP	
Metal / metal	Nickel / GFRP	Engine air intakes
	Nickel / steel	Protection of parts against erosion
	Stellite / steel	Leading edges of steam turbine blades

In metallic coatings, the bonding of a sheet of metal involves a triple layer system; damage may arise as a result of erosion, separation or tearing of the metallic coating. The adhesive layer separating the coating from the substrate is of primary importance. Various tests can be summarised as follows.

Except for the soft aluminium coatings and the medium hardness Cu-Be alloy coatings, the other protection methods are better with a polyurethane glue than with an epoxy resin glue. The difference in the erosion resistance due to the adhesive cannot be explained by its shear strength, since the shear strength of polyurethane ($6 MN/m^2$) is lower than that of the epoxy resin ($25 MN/m^2$). This difference seems to be due to the shear stress τ_s. An approximate calculation has been made by considering a two-layer system in the two cases of stress: τ_{s12} for the coating/adhesive case and τ_{s23} for the adhesive/support case. Table 7.5.2.4 –10 contains the mechanical characteristics of the metals investigated and Table 7.5.2.4 – 11 gives the values of the shear stresses τ_{s12} and τ_{s23}, as well as the length of the test before rain erosion damage occured in identical conditions of impact velocity ($V \doteq 410$ m/s), droplet diameter (1.2 mm) and rain density ($\rho_{w/a} = 0.25 \times 10^{-6}$).

A comparison can be made between the metallic coatings, the silica carbide and the tungsten carbide coatings obtained by transfer, by electron bombardment, from a cathode to the cold surface of an anode, investigated by Gentner[201] (see paragraph 7.5.1.1 – b).

TABLE 7.5.2.4 – 10

Strength and Elasticity Data on the Metal Coatings Investigated by Rieger and Boche[290]

Material	Ultimate strength MN/m^2	Young modulus, E MN/m^2	Coulomb modulus, G MN/m^2	Poisson's ratio, ν
17-7 Cr-Ni steel (German 1.4310 X12	690 - 880	196,000	74,500	0.32
18-9 Cr-Ni steel (1.4301 X5)	490 - 690	"	"	"
Alloys				
Ti Al 6 V 4	980-1230	108,000	38,750	0.395
Cu-Be soft	660			
mean	834	127,500	49,000	0.3
hard	1210			
5052 Al Mg 3	225-245	68,670	24,500	0.32

TABLE 7.5.2.4 – 11

Correlation Between Erosion Life Before Damage and Erosion Shear Stresses, from Rieger and Boche[290]

Systems Coating / glue / substrate	Computed shear stresses, MN/m^2		Erosion life before damage, minutes :
	s12	s23	
Steel / Polyurethane / Steel	15	15	93
Steel / Epoxy / Steel	330	110	16
Steel / Polyurethane / GFRP	15	15	91
Steel / Epoxy / GFRP	330	42	29
Ti-A16-V4 / Polyurethane / GFRP	470	74	13

REFERENCES

1. Caine, K.E.
   et al.
   Simulated Service Evaluation of Steels for Solid-Propellant Missile Motor Cases. United States Steel Corporation, Progress Report, Project No. ARL 40.02-070(2) TD-263 May 6, 1960. Quoted and studied in Reference 9.

2. Jackson, L.R.
   Poehapsky, T.E.
   The Effect of Composition on the Fatigue Strength of Decarburized Steel. Trans. ASM, Vol. 39, p.45, 1947.

3. Ruff, P.E.
   Hot Work Toolsteel for Aircraft. Metal Progress, Vol.75 (3), p.103, March 1959.

4. Mann, J.Y.
   The Effects of "As Forged" Surfaces and Notches on the Fatigue Strength of SAE 4140 Steel (U.T.S. 140,000 lb/in²). A.R.L., Structures and Materials Note 256, Melbourne, September 1959.

5. Hankins, G.A.
   Beeker, M.L.
   The Fatigue Resistance of Unmachined Forged Steels. Journal Iron Steel Institute, Vol.126, No.2, pp.205-236, 1932.

6. Noll, G.C.
   Lipson, C.
   Allowable Working Stresses. Proc. S.E.S.A., Vol.3, No.2, pp.89-109, 1946.

7. Takeuehi, S.
   Homma, T.
   Effect of Shot-Peening on Fatigue Strength of Metals. II – Effects on Decarburized Steels. Science Rep. Research Inst. Tohoku University, Series A, Vol.11, No.1, pp.48-55, February 1959.

8. Austin, C.R.
   Effect of Surface Decarburization on Fatigue Properties of Steel. Metals and Alloys, Vol.2, No.3, pp.117-119, September 1931.

9. Warke, W.R.
   Elsea, A.R.
   The Effects of Decarburization on the Properties of Ultrahigh-Strength Steels. DMIC Memorandum 154, Batelle Memorial Institute, Columbus, Ohio, 18 June, 1962.

10. Tueker, A.W.
    Hudaeko, V.J.
    Hakkio, J.
    Part 1 by Hudaeko: *Metallurgical Aspects of Processing High-Strength Steels,* Part II by Hakkio: *Structural Problems Involving High-Strength Steels.* The Cleveland Pneumatie Tools, S.A.E. Meeting, Atlanta, 4 April 1960.

11. Frish,
    Thomsen,
    Residual Grinding Stresses in Mild Steel. Trans. ASME, pp.337-346, April 1961.

12. Nowikowsky, L.J.
    Maranehik, J.
    Field, M.
    Distortion and Residual Surface Stress in Grinding and Milling of High-Strength Steels. SAE National Aeronautieal Meeting, New-York, 1961.

13. Sauvaire, C.
    Influence des conditions d'usinage par rectification sur l'état structural et les contraintes résiduelles des surfaces usinées. Méeanique, pp.46-52, November 1968.

14. Auvinet,
    Laborde,
    Etude de l'influence des état de surface sur la tenue en fatigue de l'acier 35 NCD 16 traité pur 180 hb. Essai N° 32689, E.A.T. Toulouse, April 1964.

15. Notton,
    Auvinet,
    Etude de l'influence des états de surface et des traitements sur la fatigue de l'acier 40 CDV 20 refondu sous vide, traité pour 190 hb. Essai N° M2-7710, E.A.T. Toulouse, April 1965.

16. Notton,
    Auvinet,
    Influence du coefficient d'entaille et de l'état de surface sur la tenue en fatigue de l'alliage T-A6V. Essai N° Mo-7334, rapport partiel N° 2, E.A.T., Toulouse, August 1965.

17. Laehenaud, R.
    Etude sur l'origine des criques apparaissant sur l'acier 16 NCD 13 après protection par oxydation noire. P.V. N° 29531, Sud-Aviation, Courbevoie.

18. Anon.
    Etude des phénomènes de fissuration superficielle de l'acier 18 NC 16 après oxydation noire. FIAT, Turin, 1966.

19. Glover, W.H.
    Grinding of Spur and Helical Gears. Dans Gear Handbook, Dudley ed. p.19-17, 1962.

20. Simkowieh, E.A.
    Loria, E.A.
    Effect of Decarburization and Grinding Conditions on Fatigue Strength of 5% Cr-Mo-V Sheet Steel. ASM 42nd Annual Convention, Preprint No.185, Philadelphia, 1960.

21.   Hertz, H.   J. reine angew. Math., Vol.92, pp.156-171, 1881, Berlin.

22.   Lundberg, G.   *Dynamic Capacity of Roller Bearings.* Acta Polytechnica, Mechanical Engineering
        Palmgren, A.   Series, Vol.1, No.3, Stockholm, 1947.

23.   Reichard, D.W.   *Residual Stresses and Subsurface Hardness Changes Induced During Rolling Contact.*
        Parker, R.J.   NASA TN D-4456, NASA Langley Center, 1968.
        Zaretsky, E.W.

24.   Timoshenko, S.   *Theory of Elasticity.* 1934.

25.   Buller, H.   *Beanspruchung und Schlupf beim Rollen elasticher Walzen.* Forsch. Ing.-Wes., Vol.27,
                                    No.4, pp.121-126, 1961.

26.   Wright, G.P.   *The Influence of Fretting and Geometric Stress Concentration on the Fatigue Strength*
        O'Connor, J.J.   *of Clamper Joints.* University of Oxford, Report No.1112/70, 1970.

27.   Smith, J.O.   *Stresses due to Tangential and Normal Loads on an Elastic Solid with Application to*
        Liu, C.K.   *Some Contact Problems.* J. Applied Mechanics, Vol.20, No.2, p.157, 1953.

28.   Feng, G.C.   *Analysis of Certain Two-Dimensional Rolling and Contact Problems.* Ph. D. Thesis,
                                    University of Minnesota, USA, 1954.

29.   Caubet, J.J.   *Interaction entre le frottement et la corrosion.* Colloque CEFRACOR, March 1971,
        Amsallen, C.   CORROSION, Vol.19, No.6, October 1971.

30.   Caubet, J.J.   *Théorie et Pratique Industrielle du Frottement.* Dunod ed., Paris, 1964.

31.   Courtel, R.   *Le Frottement dans le Vide.* Annales des Mines, pp.296-303, Paris, October–November
                                    1966.

32.   Ling, F.F.   *Welding Aspects of Sliding Friction between Unlubricated Surfaces.* Air Research and
                                      Development Command, AFOSR-TR-60-117, 30 June 1950.

33.   Bowden, F.P.   Proc. Roy. Soc. A, 154, pp.640-656, 1935.
        Ridler, K.E.W.

34.   Beilby, G.   *Aggregation and Flow of Solids.* MacMillan and Co. ed., 1921.

35.   Bowden, F.P.   *Physical Properties of Surfaces: IV – Polishing, Surface Flow and the Formation of the*
        Hughes, T.P.   *Beilby Layer.* Proc. Roy. Soc. A., Vol.160, pp.575-586, 1938.

36.   Parks, J.M.   *Recrystallisation Welding.* Amer. Welding Soc., National Spring Meeting, Houston, 1963.

37.   Buckley, D.H.   *The Influence of the Atomic Nature of Crystalline Materials on Friction.* NASA TMX-
                                    52279, Lewis Research Center, Cleveland, Ohio, 1967.

38.   Desestret, A.   *Contribution à l'étude de l'action conjuguée du frottement et de la corrosion sur les aciers*
        Spahn, H.   *inoxydables.* Corrosion, Vol.19, N°4, pp.159-170, June–July 1971.
        Wagner, G.H.

39.   Kaiser,   Archiv. Eisenhüttenwesen, Vol.24, (1/2), p.43, 1953.

40.   Ben Bachir, A.   *Contribution à l'étude de l'influence de la déformation plastique sur la corrosion des*
                                    aciers dans des solutions sulfurique diluées en présence ou non de chlorures et
                                    d'inhibiteurs organiques. Thèse, Université Paul Sabatier, Toulouse, November 1975.

41.   Mauret, P.   Communication privée, Université Paul Sabatier, Toulouse, 1975.

42.   Dobinski, S.   *Nature*, Vol.138, p.31, London, 1936. Phil. Mag., Vol.23, pp.397-408, London, 1937.

43.   Branger, J.   *The Influence of Modifications of a Fatigue Loading History Program on Fatigue*
                                    Lifetime. I.C.A.F. Symposium de Miami, 1971, NASA SP-309, p.496, 1972.

44.   Bowden, F.P.   *The Friction of Clean Metals and the Influence of Adsorbed Gases. The Temperature*
        Hughes, T.P.   *Coefficient of Friction.* Proc. Roy. Soc. A, 171, pp.263-279, 1939.

122

45.	Amontons	Mémoires Acad. Roy. Sci., 206, 1699 et 96, 1704.
46.	Coloumb	Mémoires de Mathématique et de Physique de l'Académie Royale des Sciences, 161, 1785.
47.	Bowdon, F.P. Tabor, D.	*The Area of Contact between Stationary and between Moving Surfaces.* Proc. Roy. Soc. A, 169, pp.391-413, London, 1939.
48.	Maxwell, C.	*Electricity and Magnetism.* Vol.1, 6 308, 1873.
49.	Moore, A.J.W.	*Deformation of Metals in Static and Sliding Contacts.* Proc. Roy. Soc. A, 195, p.231, 1948.
50.	Archard, J.F.	*Elastic Deformation and the Laws of Friction.* Proc. Roy. Soc., Vol.243 A, p.190, 1953.
51.	Williamson, J.B.P.	*Topography of Solid Surfaces.* Interdisciplinary Approach to Friction and Wear, NASA SP 181, pp.85-142, Washington, 1968.
52.	Dyson, J. Hirst, W.	*The True Area of Contact between Solids – an Autoradiographic Study.* Proc. Roy. Soc., London, A208, p.455, 1951.
53.	Burwell, J.T. Strang, C.D.	*On the Empirical Law of Adhesive Wear.* J. Applied Physics, Vol.23, p.18.
54.	Finkin, E.	*Surface Roughness in Wear.* Wear, Vol.6, pp.293-302, July–August 1963.
55.	Rabinowicz, E. Foster, R.G.	*The Size Distribution of Wear Fragments: Effect of Surface Energy on the Wear Process.* M.I.T., Final Report AROD-2166-1, 10 April 1962.
56.	Archard, J.F. Hirst, W.	*The Wear of Metals under Unlubricated Conditions.* Proc. Roy. Soc. A236, p.397, 1956.
57.	Bisson, E.E. Anderson, W.J.	*Advanced Bearing Technology.* NASA SP 38, 1964.
58.	Sikorski, M.E.	*The Adhesion of Metals and Factors that Influence it.* Wear, Vol.7, No.2, pp.129-224, 1964.
59.	Ernst, H. Merchant, M.E.	*Surface Friction of Clean Metals – A Basic Factor in the Metal Cutting Process.* Proc. Special Summer Conf. on Friction and Surface Finish, M.I.T., June 1940.
60.	Roach, A.E. Goodzeit, C.L. Hunnicut, R.P.	*Scoring Characteristics of Thirty-Eight Different Elemental Metals in High-Speed Sliding Contact with Steel.* Trans. ASME, Vol.11, p.89, 1968.
61.	Goodzeit, C.L.	*The Seizure of Metal Pairs during Boundary Lubrication* in *Friction and Wear*, edited by R.Davies, Elsevier Publ. Co., Amsterdam, 1959.
62.	Cocks, M.	*Interaction of Sliding Metal Surface.* J. Applied Physics, Vol.33, pp.2152-2161, 1962.
63.	Antler, M.	*Processes of Metal Transfer and Wear.* Wear, Vol.7, pp.181-203, 1964.
64.	Scott, D. Seifert, W. Westcott, V.C.	*The Particles of Wear.* Scientific American, Vol.230, No.5, pp.88-97, 1974.
65.	Nakajima, K. Mizutani, Y.	*Wear*, Vol.13, p.283, 1969.
66.	Goss, G.L. Hoeppner, D.W.	*Characterization of Fretting Fatigue Damage by SEM Analysis.* Wear, Vol.24, pp.77-95, Elsevier Sequoia S.A., Lausanne, 1973.
67.	Waterhouse, R.B.	*Physics and Metallurgy of Fretting.* AGARD Specialists Meeting on Fretting in Aircraft Systems, Preprint, 11–12 October 1974.
68.	Suh, N.P.	*The Delamination Theory of Wear*, Wear, Vol.25, p.111, 1973.

69. Welsh, N.C.   *The Dry Wear of Steel*. Phil. Trans. Roy. Soc., Vol.A257, p.31, 1965.

70. Dawson, P.H.   *Wire-Wool Type Failures in 3% Cr., 0.5% Mo Steel Bearings – A Preliminary Evaluation*
     Fidler, F.   *of Some Palliatives.* Proc. Inst. Mech. Engineers., Vol.179, Pt.3J, 1964–1965.
     Rowley, P.

71. Hother-Lushington, S.   *Failure of Turbine Bearings Using Chromium Alloy Steel Journals.* Proc. Inst. Mech.
                                Engineers, Vol.180, Pt.3K, 1965–1966.

72. Zamoruev, G.M.   *Phase Changes in Steel During Friction and Wear.* Friction and Wear in Machinery,
                                Vol.11, 1956. Translated from Russian by ASME, p.196.

73. Krichevskii, Ts.R.   *The System Iron-Nitrogen at High Pressures.* Zh. F. Kh. (Journal de Physique de
     Khazanova, N.E.   Kharkov), p.21, 1947. *Iron Nitriding.* Zh. F. Kh., p.10, 1950. Quoted in Reference 72.

74. Eyre, T.S.   *The Formation of White Layers at Rubbing Surfaces.* Metals and Materials, pp.435-439,
     Baxter, A.   October 1972.

75. Trent, E.M.   J. Iron Steel Inst., Vol.143, p.401, 1941.

76. Steininger, Z.   *Wire Industry*, Vol.34, p.583 and 761, 1967.
     Krczemniski, A.

77. Snair, W.H.   Trans. Amer. Soc., Metals, Vol.27, p.608, 1939.
     Wood, W.P.

78. Grozin, B.V.   *Développement d'une théorie du frottement et de l'usure.* (In Russian) Akad. Nauk.,
                                p.158, Moscou, 1957.

79. Rogers, M.D.   *Tribology*, Vol.2, p.123, 1969.

80. Savitskiy, K.V.   Phys. Met. Metalloved, Vol.17, p.5, 1964.
     Kogan, Yu.I.
     Kudrina, M.P.

81. Brainin, I.Ye.   Phys. Met. Metallogra, Vol.15, p.135, 1963.
     Selezneve, N.N.

82. Embury, J.D.   *Srtengthening Methods in Crystals.* Ed. Kelly and Nicholson, Elsevier Publishing Co.,
                                United Kingdom, Chapter 6, pp.331-397.

83. O'Brien, J.L.   Amer. Soc. Mechan. Engrs., Paper 65-WA/CF-1, 1965.
     King, A.H.

84. Scott, D.   Amer. Soc. Mechan. Engrs., Paper 65-WA/SF-4, 1965.
     Loy, B.
     Eberhardt, A.D.

85. Krushchov, M.M.   *Resistance of Metals to Wear by Abrasion as Related to Hardness.* Proc. Conf. on
                                Lubrication and Wear, pp.655-659, Inst. Mech. Engineers, London, 1951.

86. Kruschov, M.M.   *The Effect of Heat Treatment and Work Hardening on the Resistance to Abrasive Wear*
     Babichcv, M.A.   *of some Alloy Steels.* Friction and Wear in Machinery, Vol.19, 1964. Translated from
                                Russian by ASME. pp.1-15.

87. Larsen-Badse, J.   *The Abrasion Resistance of some Hardened and Tempered Carbon Steels.* Trans.
                                Metallurgical Society, Institute of Mining, Metallurgical and Petroleum Engineers,
                                Vol.236, pp.1461-1466, 1966.

88. Krushchov, M.M.   *Correspondence between the Relative Abrasive-Wear Resistance of Metals, Alloys, and*
     Babichev, M.A.   *some Materials and their Moduli of Elasticity.* Friction and Wear in Machinery, Vol.17,
                                1962. Translated from Russian by ASME, pp.1-8.

89. Babichcv, M.A.   *Investigation of the Abrasive Wear of Metals by the Brinell Method.* Friction and
                                Wear in Machinery, Vol.14, 1960. Translated from Russian by ASME, pp.1-29.

124

90. Nathan, G.K.
Jones, W.J.D.
The Empirical Relationship between Abrasive Wear and the Applied Conditions. Wear, Vol.9, pp.300-309, 1966.

91. Avient, B.W.E.
Goddard, J.
Wilman, H.
An Experimental Study of Friction and Wear during Abrasion of Metals. Proc. Roy. Soc., London, A258, pp.159-180, 1960.

92. Lomakin, V.S.
Investigation of Wear of Sleeves and Piston Rings of Mud Pumps. Friction and Wear in Machinery, Vol.11, 1956. Translated from Russian by ASME, pp.39-68.

93. Kosterin, lu.l.
Kragel'skii, l.V.
Relaxation Oscillations in Elastic Friction Systems. Friction and Wear in Machinery, Vol.12, 1958. Translated from Russian by ASME, pp.111-134.

94. Maratray, M.F.
L'expérimentation et l'usure des équipements. Aciers Spéciaux, N° 10, 1969. Editions S.E.M.A.S., Paris.

95. Norman, T.E.
Loeb, C.M.
Wear Tests in Grinding Balls. Trans. A.1.M.E., Vol.176, pp.490-526, 1945.

96. Borik, F.
Sponseller, D.L.
Gouging Abrasion Tests for Materials used in Ore and Rock Crushing. Part I – Description of the Test. Part II – Effect of Metallurgical Variables. ASTM Journ. of Materials, Vol.6, No.3, pp.576-605, 1971.

97. Borik, F.
Scholz, W.G.
Gouging Abrasion Test for Materials Used in Ore and Rock Crushing: Part II – Effect of Metallurgic Variables. Jour. Materials, Vol.8, No.3, pp.590-605, 1971.

98. Blok, H.
Températures des surfaces dans les conditions de graissage sous extrême pression. Laboratoire de Royal Dutch Shell, Delft, 1937, paper to the 2nd Mundial Cong   of Petroleum, Vol.3, pp.471-486, Paris, 1937.

99. Blok, H.
Measurement of Temperature Flashes on Gear Teeth under Extreme-Pressure Conditions. Proc. General Discussion on Lubrication, Int. Mech. Engrs., pt.2, pp.14-20, 1937.

100. Nieman, G.
Lechner, G.
The Measurement of Surface Temperatures on Gear Teeth. Trans. ASME, J. Basic Engineering, Vol.87D, pp.641-651, 1965.

101. Meng, V.V.
Investigation of Steel Seizure on a Roller Testing Machine (in Russian). Friction and Wear in Machinery, Vol.14, 1960. Translated from Russian by ASME, pp.202-217.

102. Blok, H.
Lubrication as a Gear Design Factor. Proc. Intern. Conf. Gearing, Inst. Mech. Engrs. pp.144-158, 1958.

103. Dyson, A.
Naylor, H.
Application of the Flash Temperature Concept to Cam and Tappet Wear Problems. Proc. Inst. Mech. Engrs., Automotive Division, p.255, 1961.

104. Naylor, H.
Cam and Friction Drives. Proc. Third Intern. Conf. Lubrication and Wear, Inst. Mech. Engrs., pp.66-76, 1967.

105. Charron, F.
Partage de la chaleur entre deux corps frottants. Pub. Sci. Techn. Air, No.182, Blondel La Rougerie ed. Paris, 1943.

106. Churchill, R.V.
Modern Operational Mathematics in Engineering. McGraw-Hill Book Co., 1944.

107. Blok, H.
The Postulate About the Constancy of Scoring Temperature. P.212, eq.(18). NASA SP-237, Interdisciplinary Approach to Lubrication of Concentrated Contacts, 1970.

108. Shipley, E.E.
Loaded Gears in Action. In *Gear Handbook*, edited by D.W.Dudley, McGraw-Hill Book, First edition, pp.14-43, 1962.

109. Way, S.
Pitting due to Rolling Contact. Trans. ASME, Vol.57, p.A-49, 1935.

110. Littmann, W.E.
Widner, R.L.
Propagation of Contact Fatigue from Surface and Subsurface Origins. Trans. ASME, Journ. of Basic Engineering, pp.624-636, September 1966.

111. Littmann, W.E.
Widner, R.L.
Wolfe, J.O.
The Role of Lubrication in Propagation of Contact Fatigue Cracks. Trans. ASME, Journal of Lubrication Technology, Paper No.67-Lub-2, Lubrication Conference, Chicago, October 17–19, 1967.

112.	Nenediet, G.H.	*Gears*, Chapter 20 of *Standard Handbook of Lubrication Engineering*, edited by O'Connor, J.J., Boyd, J. and Avallone, E.A., McGraw-Hill Book Co., 1968.
113.	Barrois, W.	*Manual on Fatigue of Structures – Fundamental and Physical Aspects*. AGARD MAN 8-70, Paris, 1970.
114.	Barrois, W.	*Fiabilité des Structures en Fatigue Basée sur l'Utilisation des Résultats des Essais, Première Partie: Bases de la Fiabilité et de la Fatigue*. L'Aéronautique et l'Astronautique, No.66, Paris, October 1977.
115.	Dang-Tran, T. Faure, L.	*Calcul de la résistance des roues cylindriques d'après les méthodes ISO et AGMA. Calcul de la pression maximale*. CETIM-Informations, pp.24-32, June 1973.
116.	Henriot, G.	*Traité Théorique et Pratique des Engrenages – I, Théorie et Technologie*. Dunod ed., 572 pages, Paris, 1968.
117.	Wellauer, E.J.	*Load Rating of Gears*, Chapter 13 of *Gear Handbook*, edited by D.W.Dudley, McGraw-Hill Book Co., 1962.
118.	Palmgren, A.	*Ball and Roller Bearings*. SKF Industries Inc., Philadelphia, 1945.
119.	Stribeck, R.	*Kugelager für belietige Belastungen*. ZVDI, Bd 45, pp.73-118, 1901.
120.	Tabor, D.	*The Hardness of Metals*. Oxford University Press, London, 1951.
121a.	Hausseguy, L. Martinod, H.	*Influence de la contrainte sur la limite élastique hertzienne*. La Recherche Aéronautique, No.37, January–February 1954.
121b.	Pomey, J. et al.	Métaux-Corrosion-Industries, Vol.26, p.313, Paris, September 1951.
122.	Sines, G. Carlson, R.	ASTM Bulletin, TP 31, p.180, February 1952.
123.	Jones, A.B.	*Analysis of Stresses and Deflections*. New Departure Division. General Motors Corporation, Bristol, Conn., USA, 1946.
124.	Anon.	*American Standard Method of Evaluating Load Ratings for Ball and Roller Bearings*. B 3.11, 1959, American Standards Association, N.Y., January 6, 1959.
125.	Gilette, C.R. Ruley, B.T.	*Rolling Elements*, Chapter 6 of *Standard Handbook of Lubrication Engineering*, edited by O'Connor, Boyd and Avallone, McGraw-Hill Book Co., 1968.
126.	Styri, H.	*Fatigue Strength of Ball Bearing Races and Heat-Treated 52100 Steel Specimens*. Proc. ASTM, Vol.51, p.682, 1951.
127.	Gumbel, E.J.	*Statistical Theory of Extreme Values and some Practical Applications*. Nat. Bur. Standards, Appl. Math., Series 33, 1954.
128.	Weibull, W.	*A Statistical Representation of Fatigue Failure in Solids*. K. Tekn. Högsk. Handl. No.26, 1949.
129.	Benard, A. Bos-Levenbach, E.D.	*The Plotting of Observations on Probability Paper*. Statistica, Vol.7, p.163, 1953.
130.	Gumbel, E.J. Carlson, P.G.	*Extreme Values in Aeronautics*. J. Aeronautical Sciences, June 1954.
131.	Tallian, T.	*Weibull Distribution of Rolling Contact Fatigue Life and Deviations Therefrom*. Trans. ASLE, Vol.5, No.1, pp.183-196, April 1962.
132.	Freudenthal, A.M. Gumbel, E.J.	*Le phénomène de la "vie minimum" en fatigue sous contraintes constantes ou variables*. Revue de Métallurgie, LVI, No.3, pp.295-298, 1959.
133.	Lipson, C. Sheth, N.J.	*Prediction of Per Cent Failures from Stress/Strength Interference*. Soc. of Automotive Engineers, Detroit Congress, Paper No.680084, January 1968.

126

134. Taylor, J.   *Manual of Aircraft Loads.* AGARD, Pergamon Press, 1965.

135. Johnson, L.G.   (a) *Statistical Prediction Techniques for Analysis of Field Failures.* Soc. of Automotive
                                Engineers, Automotive Engineering Congress, Detroit, Paper 660062, January 1966.
                                (b) *The Statistical Treatment of Fatigue Experiments.* Elsevier Publishing Co., New
                                York, 1964.

136. Anderson, W.J.   *Rolling-Element Bearings.* Machine Design, Design Data, Bearing Reference Issue,
      Zaretsky, E.V.   p.23, June 13, 1968. This paper contains a comprehensive discussion on technology
                                and selection of ball or roller bearings for various uses.

137. Kaufman, H.N.   *Analysis of Load-Type Damage by Examination of Ball Paths.* In *"Standard Handbook
                                of Lubrication Engineering"*, edited by O'Conner, Boyd and Avallone, McGraw-Hill
                                Book Co., 1968.

138. Shaw, M.C.   *Analysis and Lubrication of Bearings*, p.399, McGraw-Hill Book Co., 1949.
      Macs, E.F.

139. Palmgren, A.   *Die Lebensdauer von Kugellagern.* VDI-Z, No.68, pp.339-341, 1924.

140. Miner, M.A.   *Cumulative Damage in Fatigue.* Journal Applied Mechanics, No.12, pp.A159-164, 1945.

141. Barrois, W.   *Use of General Fatigue Data in the Interpretation of Full-Scale Fatigue Tests.* AGARD-
                                AG-228, Paris, October 1977.

142. Barrois, W.   *Stresses and Displacements due to Load Transfer by Fasteners in Structural Assemblies.*
                                Engineering Fracture Mechanics. Vol.10, pp.115-176, Pergamon Press, 1978.

143. Reichenbach, G.S.   *The Importance of Spinning Friction in Thrust-Carrying Ball Bearings.* Trans. ASME
                                Journal of Basic Engineering. pp.295-301. June 1960.

144. Andreani, C.J.   Discussion of Reference 143. He relates experienced gained due to investigations
                                sponsored by Pratt and Whitney, Aircraft Division, West Harford, Conn., USA.

145. Weibull, W.   (a) *A Statistical Theory of the Strength of Materials.* Proceedings No.151. Roy.
                                Ingeniors Vetenskaps Akademien, Stockholm, 1939.
                                (b) *The Phenomenon of Rupture in Solids.* Proc. No.153. Roy. Ingeniors Vetenskaps
                                Akadamien, Stockholm, 1939.

146. Rumbarger, J.H.   *Dynamic Capacity of Oscillating Rolling Element Bearings.* Trans. ASME, Journal of
      Jones, A.B.   Lubrication Technology, Paper No.67, Lub.22, 1967.

147. Tawresey, J.S.   *An Experimental Investigation of the Fatigue Life and Limit Load Characteristics of
      Shugarts, W.W., Jr   Needle Roller Bearings Under Oscillating Load Conditions.* Technical Documentary
                                Report No. SEG-TDR-64-4, Franklin Institute Laboratories, (AD 437 467), March
                                1964.

148. Mundt, R.   *Riffelbildung bei Wälzlagern als Folge von Stillstandserschütterungen.* VDI-Z. 105,
      Pitroff, H.   No.26, (11), September 1963.

149. Tomlinson, G.A.   *Investigation of the Fretting Corrosion of Closely Fitting Surfaces.* Proc. Inst. Mech.
      Thorpe, P.L.   Engineers, 141, pp.223-249, 1939.

150. Sakmann, B.W.   *An Investigation of Fretting Corrosion Under Several Conditions of Oxidation.* NACA
      Rightmire, B.G.   T.N. No.1492, Washington, D.C., 1948.

151. Carter, F.W.   *On the Action of a Locomotive Driving Wheel.* Proc. Roy. Soc., A112, pp.151-157,
                                London, 1926.

152. Johnson, K.L.   *Tangential Tractions and Microslip in Rolling Contact.* Rolling Contact Phenomena.
                                J.B.Bidwell ed., Elsevier Press, pp.6-28, 1962.

153. Poritsky, H.   *Stresses and Deflections of Cylindrical Bodies in Contact.* J. Applied Mechanics, ASME,
                                Vol.17, pp.191-201 and pp.465-468, 1950.

154. Poritsky, H.   *Microslip and Creep in Contacts.* *"Interdisciplinary Approach to the Lubrication of
                                Concentrated Contacts".* NASA SP-237. pp.77-152. Washington, D.C., 1970.

155. Moreau, M.
     Gostoli, M.
Le fretting-corrosion et les dégradations dues aux actions de contact. Matériaux et Techniques, pp.385-391, November 1976.

156. Almen, J.O.
Lubricants and False Brinelling of Ball and Roller Bearings. Mech. Engng., 59, p.415, 1937.

157. Disapio, A.
Solid and Bonded-Film Lubricants. Machine Design, Bearing Reference Issue, Chapter 7, pp.59-62, June 1968.

158. Moreau, M.
Private Communication.

159. Hoeppner, D.W.
     Goss, G.L.
Research on the Mechanism of Fretting Fatigue. Corrosion Fatigue, NACE-2, pp.617-626, NACE, Houston, Texas, 77001, 1972.

160. Feng, I.M.
     Uhlig, H.H.
Fretting Corrosion of Mild Steel in Air and Nitrogen. J. Applied Mechanics, Vol.21, No.4, pp.395-400, December 1954.

161. Wright, K.H.
An Investigation of Fretting Corrosion. Proc. Inst. Mech. Engineers, Vol.18, p.556, 1952-53.

162. Feng, I.M.
     Rightmire, B.G.
The Mechanism of Fretting. Lubrication Engineering, Vol.9, p.134.

163. Uhlig, H.H.
Mechanism of Fretting Corrosion. J. Applied Mechanics, Vol.21, No.4, p.401, December 1954.

164. Bailey, J.M.
     Godfrey, D.
Coefficient of Friction and Damage to Contact Area During the Early Stages of Fretting. II – Steel, Iron, Iron Oxide, and Glass Combinations. NACA TN 3144, April 1954.

165. Brainard, W.A.
     Buckley, D.H.
Adhesion, Friction and Wear of a Copper Bicrystal with (111) and (210) Grains. NASA TN D-7232, 1973.

166. Pepper, S.V.
     Buckley, D.H.
Metallic Transfer between Metals in Sliding Contact Examined by Auger Emission Spectrography. NASA TN D-6716, March 1972.

167. Buckley, D.H.
Oxygen and Sulfur Interactions with a Clean Iron Surface and the Effect of Rubbing Contact on these Interactions. NASA TN D-7283, May 1973.

168. Buckley, D.H.
Friction, Wear, and Lubrication in Vacuum. NASA SP-277, 1971.

169. Tallian, T.E.
On Completing Failure Modes in Rolling Contact. ASLE Trans., Vol.10, pp.418-439, 1967.

170. Martin, J.A.
     et al.
Second Summary Report on Structural Studies of Bearing Steel Undergoing Cyclic Stressing. Office of Naval Research, SKF Report AL66M031, DDC. AD 482 896, 1965.

171. Martin, J.A.
     Borgese, S.F.
     Eberhardt, A.D.
Microstructural Alterations of Rolling Bearing Steel Undergoing Cyclic Stressing. J. Basic Eng. 88, pp.555-567, 1967.

172. Martin, J.A.
     et al.
First Summary Report on Structural Studies of Bearing Steel Undergoing Cyclic Stressing. Office of Naval Research, SKF Report AL65M030, AD 462 896, 1965.

173. Barrois, W.
Théorie de l'évolution des métaux pendant la fatigue. Revue de Métallurgie, No.8, LV, pp.761-777, 1958.

174. Barrois, W.
See Reference 113.

175. Barrois, W.
Fiabilité des Structures en Fatigue, Basée sur l'Utilisation des Résultats des Essais. Second Part, L'Aéronautique et l'Astronautique, No.67, pp.39-56, December 1977. See Reference 114 for the first part.

176. Muro, H.
     Tshushima, T.
     Nagafuchi, M.
Initiation and Propagation of Surface Cracks in Rolling Fatigue of High Hardness Steel. Wear, Vol.35, No.2, pp.261-282, 1975.

177. Zaretsky, E.V.
     Parker, R.J.
     Anderson, W.J.
A Study of Residual Stresses Induced During Rolling. NASA Technical Memorandum TM X-52422. Conference "Lubrication" of ASME and ASLE, Atlantic City, New Jersey, October 1968.

128

178.   Moore, M.B.   *An Investigation of the Mechanism of Erosion by Impingement.* Progress Report Doc. NY0-3477-11, Atomic Energy Commission, Rutgers — The State University, New Brunswick, N.J. 08903, Abstract N-68-12361, June 1967.

179.   Bévalot, J.   *Precèdés Mécanique d'Amélioration de l'Etat de Surface et de la Tenue en Fatigue par Projection de Billes de verre et par Coïnage.* Société A.M.D.-B.A. Doc. D.G.T. No.11079, February 1975, not published.

180.   Finnie, I.   *Erosion by Solid Particles in a Fluid Stream.* ASTM STP 307, pp.70-82, 1962.

181.   Bovet, T.   *Etude de l'érosion par le sable dans les turbines hydrauliques.* Bulletin Technique de la Suisse Romande, No.3, pp.37-49, February 1958.

182.   Stauffer, W.A.   *Wear of Metals by Sand Erosion.* Metal Progress, pp.102-107, January 1956.

183.   Leith, W.C.   *Accelerated Cavitation Erosion and Sand Erosion.* ASTM STP 307, pp.46-69, 1962.
       Mellquham, W.G.

184.   Mathieson   Quoted in Reference 183.
       Hobbs

185.   Patel, D.   *Erosion Process as Influenced by Surface Hardeners.* Master of Science Thesis, Washington State University, 1968.

186.   Sheldon, G.L.   *Effects of Surface Hardness and Other Material Properties on Erosion Wear of Metals by Solid Particles.* ASME publication, Paper No.76-WA/Mat-8, Meeting ASME, New York, December 1976.

187.   Hutchings, I.M.   *Prediction of the Resistance of Metals to Erosion by Solid Particles.* Wear, Vol.35, No.2, pp.371-374, December 1975.

188.   Finnie, I.   *Erosion of Metals by Solid Particles.* Journal of Materials, Vol.2, No.3, pp.682-700,
       Wolak, J.   1967.
       Kabil, Y.

189.   Ascarelli, P.   *Relation Between the Erosion by Solid Particles and the Physical Properties of Metals.* US Army, Materials Res. Center, Techn. Report 71-47, 1971.

190.   Tadolder, Y.A.   *Influence of Abrasive Grain Geometry on the Solid Particle Erosion of Metals.* Tr. Tallin Politekh. Inst., Series A, No.237, pp.15-22, 1966.

191.   Sheldon, G.L.   *Similarities and Differences in the Erosion Behavior of Materials.* Trans. ASME, J. Basic Engineering, Vol.92, p.619, 1970.

192.   Tilly, G.P.   *The Interaction of Particles and Material Behavior in Erosion Processes.* Wear, Vol.16,
       Sage, W.   p.447, 1970.

193.   Goodwin, J.E.   *A Study of Erosion by Solid Particles.* Proc. Inst. Mech. Engrs., 184(15), p.279, 1969.
       Sage, N.
       Tilly, G.P.

194.   Sheldon, G.L.   *An Investigation of Impingement Erosion using Single Particles.* Wear, Vol.21,
       Kanhere, A.   pp.195-209, 1972.

195.   Sheldon, G.L.   *On the Ductile Behavior of Nominally Brittle Materials during Erosive Cutting.* Trans.
       Finnie, I.   ASME, Series B, J. Eng. Ind., Vol.89, p.387, 1966.

196.   Sheldon, G.L.   *Erosion of Brittle Materials.* Dr Engr. Dissertation, University of California, 1965.

197.   Behrendt, A.   *Solid Impact.* 3rd Intern. Conference on Rain Erosion and Associated Phenomena, pp.797-820, edited by Fyall and King, R.A.E. Farnborough, England, 1970.

198.   Behrendt, A.   *Sand Erosion of Dome and Window Materials.* 4th Int. Conf. on Rain Erosion and Related Phenomena, pp.845-861, edited by Fyall and King, R.A.E., 1974.

199.   Tuitt, D.A.   *Erosion Tests of Metallic Coatings.* 4th Int. Conf. on Rain Erosion, pp.677-699.

200. Alderson, M.   *A Preliminary Investigation into the Behavior of Thin Metal Sheets Subject to Solid Particle Erosion*. 4th Int. Conf. on Rain Erosion, pp.863-885, 1974.

201. Gentner, K.   *Thin, Erosion Resistant Coatings, Deposited by Means of Sputtering Techniques*. 4th Int. Conf. on Rain Erosion, pp.701-713, edited by Fyall and King, R.A.E., 1974.

202. Engel, O.G.   (a) *Pits in Metals Caused by Collision with Liquid Drops and Soft Metal Spheres*. Nat. Bur. Standards, Journal of Research, Vol.62, p.229, 1959.
(b) *Pits in Metals Caused by Collision with Liquid Drops and Rigid Steel Spheres*. Nat. Bur. Standards, Journal of Research, p.29, 1960.
(c) *Impact of Liquid Drops*. ASTM STP 307, pp.3-16, 1962.
(d) *Basic Research on Liquid-Drop-Impact Erosion*. NASA Cr-1559, from General Electric Co., Cincinnati, Ohio, for Lewis Research Center, 1970.

203. Saint-Venant, B. de   Journal de Mathématiques Pures et Appliquées, 2ème Série, Vol.12, 1867.

204. Clark, D.S. / Wood, D.S.   *The Time Delay for the Initiation of Plastic Deformation at Rapidly Applied Constant Stress*. Proc. ASTM, Vol.49, pp.717-735, 1949.

205. Graham, O.   *An Investigation into the Mode of Metal Removal in the Grinding Process*. Wear, Vol.19, p.301, 1972.

206. Sullivan, R.C. et al.   *Influence of Particle Size and Velocity on Crater Depth*. 3rd Int. Conf. on Rain Erosion, pp.777-795, Fyall and King ed. RAE Farnborough, 1970.

207. Denardo et al.   *Projectile Size Effects on Hypervelocity Impacts Craters in Aluminium*. NASA TN D-4067.

208. Adler, W.F.   *Erosion of Fused Silica by Glass Beads*. ASTM STP 567, pp.294-314, 1974.

209. Tsai, Y.M.   Intern. Journal of Solids and Structures, Vol.7, pp.543-558, 1971.

210. Fyall, A.A.   *Single Impact Studies with Liquids and Solids*. 2nd Intern. Conf. on Rain Erosion, pp.563-591, Fyall and King ed. RAE Farnborough, 1967.

211. Brunton, J.H.   Discussion of the Reference 210.

212. Levy, M. / Morossi, J.L.   *Erosion and Fatigue Behavior of Coated Titanium Alloys for Gas Turbine Compressor Applications*. Army Material and Mechanics Research Center Watertown, February 1976.

213. Heymann, F.J.   *Erosion by Liquids... the Mysterious*. Machine Design, Vol.42, No.30, pp.118-124, December 1970.

214. Hammitt, F.G.   *Damage due to Cavitation and Subcooled Boiling Bubble Collapse*. Proc. Inst. Mech. Engineers, Vol.183, Pt.1(2), pp.31-50, 1968–1969.

215. Thiruvengadam, A.   *The Concept of Erosion Strength*. ASTM STP 408, pp.22-41, Philadelphia, Pa., 1967.

216. Thomas, G.P.   *Multiple Impact Experiments and Initial Stage of Deformation*. In "Deformation of Solids by the Impact of Liquids". The Roy. Soc., London, May 1965.

217. Marriott, J.B. / Rowden, G.   *The Deformation of Steam Turbine Materials by Liquid Impact*. Phil. Trans. Roy. Soc., A. 260, 144, 1965.

218. DeCorso, S.M. / Kothmann, R.E.   *Erosion by Liquid Impact*. In: "Erosion and Cavitation". ASTM STP 307, pp.32-45, 1962.

219. Hoff, G. / Langbein, G. / Rieger, H.   *Material Destruction Due to Liquid Impact*. ASTM STP 408, Philadelphia, Pa., 19103, 1967.

220. Fyall, A.A. / King, R.B. / Strain, R.N.C.   *Rain Erosion Aspects of Aircraft and Guided Missiles*. Journ. Royal Aeron. Soc., p.447, 1962.

221. Schmitt, G.F., Jr   *Influence of Velocity, Impingement Angle, Heating, and Aerodynamic Shock Layers*
      Reinecke, W.G.   *on Erosion of Materials at Velocities of 1700 m/s.* ASTM STP 567, pp.219-238,
      Waldman, G.D.   Philadelphia, Pa 19103, USA, 1974.

222. Schmitt, G.F., Jr   *Erosion Rate-Velocity Dependence for Materials at Supersonic Speeds.* ASTM
                          STP 474, pp.323-352, 1970.

223. Rochester, M.C.   *Influence of Physical Properties of the Liquid on the Erosion of Solids.* ASTM
      Brunton, J.H.   STP 567, pp.128-147, 1974.

224. Rochester, M.C.   *Surface Pressure Distribution During Drop Impingement.* 4th Intern. Conf. on Rain
      Brunton, J.H.   Erosion and Related Phenomena. Ed. RAE Farnborough, Meersburg, 1974.

225. Bowden, F.P.   *Damage to Solids by Liquid Impact at Supersonic Speeds.* Nature, Vol.181, pp.873-875,
      Brunton, J.H.   1958.

226. Hammit, F.G.   *Liquid Impact Behaviour of Various Non Metallic Materials.* ASTM STP 567,
      et al.   pp.197-218, 1974.

227. Johnson, W.   *Transient Stress Distribution Caused by Water Jet Impact.* Journal Mech. Engineering
      Vickers, G.W.   Science, Vol.15, 4, 1973.

228. Kinslow, R.   *Supersonic Liquid Impact of Solids.* 4th Intern. Conf. on Rain Erosion, pp.271-293,
                          ed. by Fyall and King, RAE Farnborough, Meersburg, 1974.

229. Huang, Y.C.   Report UMICH 03371-9-T, 1970 and 033710-10-T, 1971, Michigan University, Ann
      Hammitt, F.G.   Arbor, Mich. 48105.
      Yang, W.J.

230. Heymann, F.   *A Survey of Clues to the Relationship Between Erosion Rate and Impact Parameters.*
                          2nd Intern. Conf. on Rain Erosion, pp.683-760, ed. RAE Farnborough, 1967.

231. Morris, J.W.   *The Rain Erosion of Aluminium at Supersonic Velocity.* 3rd Intern. Conf. on Rain
      Bates, C.H.   Erosion, pp.261-301, Fyall and King ed., RAE Farnborough, 1970.
      Wahl, N.E.

232. Rice, M.H.   *Equation of State for Water to 250 Kilobars.* J. Chem. Phys., Vol.26, No.4, pp.824-830,
      Walsh, J.M.   April 1957.

233. Cook, M.A.   *Erosion Tests of Steam Turbine Blade Materials.* Proc. ASTM, Vol.64, pp.782-796,
      Keyes, R.T.   1964.
      Ursenbach, W.O.

234. Brunton, J.H.   *The Flow of a Liquid Drop During Impact.* 3rd Intern. Conf. on Rain Erosion,
      Camus, J.J.   pp.327-352, Fyall and King ed., RAE Farnborough, 1970.

235. Abrahamson, G.R.   *Permanent Periodic Surface Deformations due to a Travel in Jet.* J. Applied Mechanics,
                          pp.519-528, December 1961.

236. Bahrani, A.S.   Proc. Inst. Mech. Engineers, Vol.179, p.264, 1965.
      Crossland, B.

237. Rayleigh, Lord   Philosophical Magazine, Vol.54, pp.94-100, London, 1917.

238. Barclay, F.J.   Discussion of the Reference 214 (Hammitt).
      Ledwige, T.J.
      Confield, G.C.

239. Brunton, J.H.   *Cavitation Damage.* 3rd Intern. Conf. on Rain Erosion, pp.821-846, Fyall and King ed.,
                          RAE Farnborough, 1970.

240. Vyas, B.   *Cavitation-Induced Deformation of Aluminium.* ASTM STP 567, pp.77-105, 1974.
      Preece, C.M.

241. Laurent, P.   Publication Scientifique No.256 du Ministère de l'Air, Thèse, Paris, 10 January, 1951.

242. Heymann, F.J. *On the Time Dependence of the Rate of Erosion due to Impingement or Cavitation.* ASTM STP 408, pp.70-100, 1967.

243. Plesset, M.S. *Effect of Exposure Time on Cavitation Damage.* Trans. ASME, Vol.88D, No.4, Devine, R.E. pp.691-705, 1966.

244. Beckwith, D.J. *Factors Affecting Erosion in a 12% Chromium Steel.* 2nd Intern. Conf. on Rain Erosion, Marriott, J.B. pp.761-784, Fyall and King ed., RAE Farnborough, 1967.

245. Hoff, G. *Rain and Sand Erosion, Phenomena of Material Destruction Caused by Repeated Loads.* Herbert, W. ASTM STP 474, pp.353-382, 1970. Rieger, H.

246. Schütz, W. L.B.F. Technische Mitteilungen T.M. 17, 1965, T.M.20 and T.M.21, 1967.

247. Gould, G.C. *Cavitation-Erosion of Stellite and Other Metallic Materials.* 3rd Intern. Conf. on Rain Erosion, pp.881-906, Fyall and King ed., RAE Farnborough, 1970.

248. Smith, A. *Erosion of Steam Turbine Blade Shield Materials.* ASTM STP 408, pp.125-158, 1967. Kent, R.P. Armstrong, R.L.

249. Thiruvengadam, A. *Experimental and Analytic Investigation on Liquid Impact Erosion.* ASTM STP 474, Rudy, S. pp.249-287, 1970. Gunasekeran, M.

250. Schulmeister, R. *Vibratory Tests in Water on the Combined Action of Cavitation and Corrosion.* ASTM STP 474, pp.109-126, 1970.

251. Kallas, D.H. *Corrosion, Wear and Erosion – An Ancient Art and a Modern Science.* ASTM STP 567, pp.1-17, 1974.

252. Parsons, C.A. Engineering, Vol.107, pp.515-519, 1919. Cook, S.S.

253. Preiser, H.S. Corrosion, Vol.7, pp.535t-549t, 1961. Tytell, B.H.

254. Lichtman, J.Z. *Handbook on Corrosion Testing and Evaluation.* W.H.Ailor ed., pp.453-472, Wiley, Kallas, D.H. New-York, 1971. Ruffolo, A.

255. Waring, S. Journal of Ship Research, Vol.9, December 1965. Preiser, H.S. Thiruvengadam, A.

256. McGuinness, T. *Cavitation Erosion – Corrosion Modeling.* ASTM STP 567, pp.30-55, 1974. Thiruvengadam, A.

257. Schulmeister, R. *Über die Wirkung von Korrosion-Schutz-Mitteln auf die Werkstoffzerstörung durch Cavitation und Korrosion.* Dissertation T.H. Darmstadt D 17, 1966.

258. Oelert, W. *Kühlwasserbehandlung bei schellaufenden Dieselmotoren.* MTZ, Vol.29, No.6, pp.240-248, 1968.

259. Lichtman, J.Z. In discussion of Reference 256.

260. Steller, K. *Effects of Cavitation on Materials in Field and Laboratory Conditions.* ASTM STP 567, Krzysztofowies, T. pp.152-170, 1974. Reymann, Z.

261. Van der Horst, J.M.A. *Erosion-Corrosion of Finned Heat Exchanger Tubes.* ASTM STP 567, pp.18-29, 1974. Sloan, C.R.

262. Rheingans, W.J. *Cavitation in Hydraulic Turbines.* ASTM STP 307, pp.17-31, 1962.

263. Rheingans, W.J. *Cavitation Damage.* ASME, Cavitation Symposium, 1956.

132

264.   Rieger, H.   *Comparative Investigation on Erosion Caused by Drop Impact and Cavitation.* 2nd Intern. Conf. on Rain Erosion, pp.793-822, ed by Fyall and King, RAE Farnborough, Meersburg, 1967.

265.   Speidel, M.O.   *Resistance to Rain Erosion, Stress-Corrosion Cracking and Corrosion-Fatigue in a 12%*
       Keser, H.C.   *Chromium Steel.* 4th Conf. on Rain Erosion, pp.571-549, 1974.

266.   Hyatt, M.V.   *Use of Precracked Specimens in Stress-Corrosion Testing of High-Strength Aluminium Alloys.* The Boeing Company, Report D6-24466, November 1969.

267.   Anon.   Military Standardization Handbook: *The Stress-Corrosion Cracking and Hydrogen-Stress Cracking of Metals.* MIL-HDBK-724(MR), AMRMRC, Watertown, Massachusetss, 02172, 1 October, 1969.

268.   Gould, G.C.   *Some Observations on Erosion by Cavitation and Impingement.* ASTM STP 474, pp.182-210, 1970.

269.   Young, S.G.   *Accelerated Cavitation Damage of Steels and Superalloys in Sodium and Mercury.*
       Johnston, J.R.   ASTM STP 408, pp.186-219, 1967.

270.   Young, S.G.   *Effect of Temperature and Pressure on Cavitation Damage in Sodium.* ASTM STP 474,
       Johnston, J.R.   pp.67-102, 1970.

271.   Garcia, R.   *Correlation of Cavitation Damage with Material and Fluid Properties.* ASTM STP 408.
       Hammitt, F.G.   pp.239-283, 1967.
       Nystrom, R.E.

272.   Garcia, R.   *Ultrasonic-Induced Cavitation Studies in Mercury and Water.* ORA TR 05031-3-T,
       Hammitt, F.G.   University of Michigan, Ann Arbor, Mich., December 1965.
       Nystrom, R.E.

273.   Garcia, R.   *Ultrasonic-Induced Cavitation in Liquid Metals at 500°F.* Internal Report 05031-1-1,
       Hammitt, F.G.   Depart. Nuclear Engng, Univ. Michigan, Ann Arbor, Mich., April 1965.

274.   Garcia, R.   *Ultrasonic-Induced Cavitation Studies on Lead-Bismuth Alloy at Elevated Temperatures.*
       Hammitt, F.G.   Corrosion, Vol.22, No.6, p.157, June 1966.

275.   Hobbs, J.M.   *Cavitation Erosion in Oil Hydraulic Equipment.* Metals and Materials, Vol.6, No.1,
       McCloy, D.   pp.27-35, January 1972.

276.   Hobbs, J.M.   *Environmentally Controlled Cavitation Test.* ASTM STP 474, pp.29-46, 1970.
       Rachman, D.

277.   Kozirev, S.P.   *Analogy Between Erosion Damage and Pitting of Machine Component Surface.* ASTM STP 474, pp.409-421, 1970.

278.   Trubin, G.V.   *Kontaktnaya ustalost materialov dlia zubchatykh koles.* Mashgiz 1962.

279.   Tichler, J.W.   *A Note on the Correlation between Cavitation Erosion and Rolling Contact Fatigue*
       Scott, D.A.   *Resistance of Ball Bearing Steel.* Wear, Vol.16, 1970.

280.   Tichler, J.W.   *Time Dependence of Cavitation Erosion and the Effect of Some Material Properties.*
       de Gee, A.W.J.   3rd Intern. Conf. on Rain Erosion, pp.847-879, 1970.

281.   Tichler, J.W.   *Applied Erosion Cavitation Testing.* ASTM STP 567, pp.56-74, 1974.
       de Gee, A.W.J.
       Van Elst, H.C.

282.   Behrendt, A.   *Study of Parameters of Flight Materials at Speeds up to 1000 Meter per Second.* 4th Int. Conf. Rain Erosion, Vol.II, pp.425-448, 1974.

283.   Rieger, H.   *Investigation on the Influence of Various Test Parameters on Material Destruction at Drop Impact.* 3rd Int. Conf. Rain Erosion, pp.147-207, 1970.

284.   Schmitt, G.F., Jr   *Rain Droplet Erosion Mechanisms in Transparent Plastic Materials.* 4th Int. Conf. Rain Erosion, Vol.II, pp.455-484, 1974.

285.   Hoff, G.   *Rain Erosion of Infrared Transmitting Materials.* Proc. 11th Symposium on Electro-
       Rieger, H.   magnetic Windows, pp.93-97, Atlanta, August 1972.

286.   King, R.B.   *Multiple Impact Rain Erosion Studies at Velocities up to 450 m/s, M = 1.3.* 2nd Int.
                            Conf. Rain Erosion, pp.201-213, RAE Farnborough ed., Meersburg, 1967.

287.   Mueller, E.   *Measurement of the Simulated Rainfall at the Holloman Track Test Facility.*
       Sims, A.   AF CRL-70-028L, University of Illinois, 111, April 1970.

288.   Springer, G.S.   *Analysis of Rain Erosion of Coated Materials.* 4th Int. Conf. Rain Erosion, Vol.II,
       Yang, C.-I.   pp.601-636, 1974.
       Larsen, P.S.

289.   Engel, O.   *A Study of Composite Coating for Rain-Erosion Protection of Radomes.* 4th Int. Conf.
                            Rain Erosion, Vol.II, pp.715-766, 1974.

290.   Rieger, H.   *Erosion Behaviours of Surface Coatings.* 4th Int. Conf. Rain Erosion, Vol.II,
       Boche, H.   pp.637-675, 1974.

REPORT DOCUMENTATION PAGE

1. Recipient's Reference	2. Originator's Reference	3. Further Reference	4. Security Classification of Document
	AGARD-MAN-10 (ENG.)	ISBN 92-835-1389-4	UNCLASSIFIED

5. Originator	Advisory Group for Aerospace Research and Development North Atlantic Treaty Organization 7 rue Ancelle, 92200 Neuilly sur Seine, France

6. Title	MANUAL ON THE FATIGUE OF STRUCTURES

7. Presented at	

8. Author(s)/Editor(s)	9. Date
W.G.Barrois	June 1981

10. Author's/Editor's Address	11. Pages
Ingénieur en Chef Militaire Honoraire de l'Armement (Air) 42 rue Larmeroux, 92170 Vanves, France	140

12. Distribution Statement	This document is distributed in accordance with AGARD policies and regulations, which are outlined on the Outside Back Covers of all AGARD publications.

13. Keywords/Descriptors
Fatigue Mechanical damage Corrosion Plastic deformation

14. Abstract

The present publication (AGARD-MAN-10 (Eng.)) contains Chapter 7 which deals with mechanical surface damage. This concerns surface damage arising from wheel grinding, wear, rolling fatigue, contact fatigue, fretting fatigue and erosion by solid or liquid particles. Such damage is often the origin of fatigue cracks. An attempt is made to summarize those aspects of scientific knowledge in the field which are particularly relevant to the structural design process. It is hoped that full appreciation of this information and its careful use by designers will improve significantly the environmental resistance of our future vehicles and will thus produce important benefits in cost and maintenance reduction and in aircraft availability.

This Manual was prepared at the request of the Structures and Materials Panel of AGARD.

AGARD-MAN-10 (ENG.)		AGARD-MAN-10 (ENG.)
AGARD Manual 10 (ENG.) Advisory Group for Aerospace Research and Development, NATO MANUAL ON THE FATIGUE OF STRUCTURES W.G.Barrois Published June 1981 140 pages The present publication (AGARD-MAN-10 (Eng.)) contains Chapter 7 which deals with mechanical surface damage. This concerns surface damage arising from wheel grinding, wear, rolling fatigue, contact fatigue, fretting fatigue and erosion by solid or liquid particles. Such damage is often the origin of fatigue cracks. An attempt is made to summarize those aspects of scientific knowledge in the field which are particularly relevant P.T.O.	Fatigue Mechanical damage Corrosion Plastic deformation	AGARD Manual 10 (ENG.) Advisory Group for Aerospace Research and Development, NATO MANUAL ON THE FATIGUE OF STRUCTURES W.G.Barrois Published June 1981 140 pages The present publication (AGARD-MAN-10 (Eng.)) contains Chapter 7 which deals with mechanical surface damage. This concerns surface damage arising from wheel grinding, wear, rolling fatigue, contact fatigue, fretting fatigue and erosion by solid or liquid particles. Such damage is often the origin of fatigue cracks. An attempt is made to summarize those aspects of scientific knowledge in the field which are particularly relevant P.T.O.
Fatigue Mechanical damage Corrosion Plastic deformation		Fatigue Mechanical damage Corrosion Plastic deformation

AGARD-MAN-10 (ENG.)		AGARD-MAN-10 (ENG.)
AGARD Manual 10 (ENG.) Advisory Group for Aerospace Research and Development, NATO MANUAL ON THE FATIGUE OF STRUCTURES W.G.Barrois Published June 1981 140 pages The present publication (AGARD-MAN-10 (Eng.)) contains Chapter 7 which deals with mechanical surface damage. This concerns surface damage arising from wheel grinding, wear, rolling fatigue, contact fatigue, fretting fatigue and erosion by solid or liquid particles. Such damage is often the origin of fatigue cracks. An attempt is made to summarize those aspects of scientific knowledge in the field which are particularly relevant P.T.O.	Fatigue Mechanical damage Corrosion Plastic deformation	AGARD Manual 10 (ENG.) Advisory Group for Aerospace Research and Development, NATO MANUAL ON THE FATIGUE OF STRUCTURES W.G.Barrois Published June 1981 140 pages The present publication (AGARD-MAN-10 (Eng.)) contains Chapter 7 which deals with mechanical surface damage. This concerns surface damage arising from wheel grinding, wear, rolling fatigue, contact fatigue, fretting fatigue and erosion by solid or liquid particles. Such damage is often the origin of fatigue cracks. An attempt is made to summarize those aspects of scientific knowledge in the field which are particularly relevant P.T.O.
Fatigue Mechanical damage Corrosion Plastic deformation		Fatigue Mechanical damage Corrosion Plastic deformation

to the structural design process. It is hoped that full appreciation of this information and its careful use by designers will improve significantly the environmental resistance of our future vehicles and will thus produce important benefits in cost and maintenance reduction and in aircraft availability.

This Manual was prepared at the request of the Structures and Materials Panel of AGARD.

to the structural design process. It is hoped that full appreciation of this information and its careful use by designers will improve significantly the environmental resistance of our future vehicles and will thus produce important benefits in cost and maintenance reduction and in aircraft availability.

This Manual was prepared at the request of the Structures and Materials Panel of AGARD.

to the structural design process. It is hoped that full appreciation of this information and its careful use by designers will improve significantly the environmental resistance of our future vehicles and will thus produce important benefits in cost and maintenance reduction and in aircraft availability.

This Manual was prepared at the request of the Structures and Materials Panel of AGARD.

to the structural design process. It is hoped that full appreciation of this information and its careful use by designers will improve significantly the environmental resistance of our future vehicles and will thus produce important benefits in cost and maintenance reduction and in aircraft availability.

This Manual was prepared at the request of the Structures and Materials Panel of AGARD.